SECURITY CLASSIFICATION OF THIS PAGE (When Data Entered)

REPORT DOCUMENTATION PAGE

READ INSTRUCTIONS BEFORE COMPLETING FORM

1. REPORT NUMBER: 4 (14) TR-7
2. GOVT ACCESSION NO.
3. RECIPIENT'S CATALOG NUMBER

4. TITLE (and Subtitle): Research on Problems Related to Laser Communication through Water.

5. TYPE OF REPORT & PERIOD COVERED: Final Technical Report, Jul[redacted]73 - Dec [redacted]78.

6. PERFORMING ORG. REPORT NUMBER

7. AUTHOR(s): W.R. Bennett, Jr. [redacted] D.B. Carlin

8. CONTRACT OR GRANT NUMBER(s): ONR N00014-67-A-0097-0021

9. PERFORMING ORGANIZATION NAME AND ADDRESS: Engineering and Applied Science Dept., Yale University, New Haven, Conn. 06520

10. PROGRAM ELEMENT, PROJECT, TASK AREA & WORK UNIT NUMBERS: 9751-02, 61102F

11. CONTROLLING OFFICE NAME AND ADDRESS: ONR Administrative Contracting Office, 715 Broadway, New York, N.Y. 10003

12. REPORT DATE: Dec.7, 1978

13. NUMBER OF PAGES: 102

14. MONITORING AGENCY NAME & ADDRESS(if different from Controlling Office)

15. SECURITY CLASS. (of this report): unclassified

15a. DECLASSIFICATION/DOWNGRADING SCHEDULE

LEVEL II

16. DISTRIBUTION STATEMENT (of this Report): Approved for public release; distribution unlimited.

17. DISTRIBUTION STATEMENT (of the abstract entered in Block 20, if different from Report)

18. SUPPLEMENTARY NOTES

19. KEY WORDS (Continue on reverse side if necessary and identify by block number)
Argon ion laser
picosecond time-interval measurement
mode-locked lasers
cavity dumped lasers

20. ABSTRACT (Continue on reverse side if necessary and identify by block number)

See Following page

78 12 18 049

DD FORM 1 JAN 73 1473 EDITION OF 1 NOV 65 IS OBSOLETE S/N 0102-014-6601

SECURITY CLASSIFICATION OF THIS PAGE (When Data Entered)

AD A062443
DDC FILE COPY
DDC DEC 20 1978 F

ABSTRACT

Several of the more intense emission lines from the argon ion laser fall within the blue-green "transmission window" of sea water. Although relatively modest cw power and efficiency are obtained from argon ion lasers of practical laboratory size, the medium itself has an unusually high gain-bandwidth product when compared to other known gas laser systems. Consequently, it is possible in principle to obtain relatively high peak power pulses at high repetition frequencies from cw argon ion lasers operated in a synchronized cavity-dumped, mode-locked manner. Because such pulse chains might have practical applicability in the area of underwater communication, it seemed appropriate to investigate a number of basic physical problems associated with the production of such mode-locked laser pulse chains and with their applicability in time-interval measurement.

A number of new techniques have been developed and new physical observations have been made during the course of this research: A technique based on the two-quantum photoeffect was devised and used to study second-order intensity correlations, pulse shapes and time delays in the picosecond time domain. A method of analysis was developed for the practical design of synchronized cavity-dumped, mode-locked lasers which method is based on concepts of folded, generalized confocal equivalent cavities. Precise studies of pulse shapes from mode-locked argon ion lasers were made both with and without synchronized cavity dumping. Data were obtained for spectral distributions, peak intensities and pulse widths as a function of discharge current for such laser systems. Our results imply a pulse shape which is closely Gaussian and a laser line profile which is in good agreement with previous line broadening studies in the argon ion laser system.

Some details of the present final report have been contained in three previous interim technical reports and in three journal publications*. The full final report contained here was the basis of the PhD dissertation of D.B.Carlin in the Engineering and Applied Science Department at Yale University.

---

*W.R.Bennett,Jr., D.B.Carlin and G.J.Collins, IEEE J.Quant. Elect. Vol. QE-10, p.97 (1974).
D.B.Carlin and W.R.Bennett,Jr., Appl. Opt. Vol.15, p.2020 (1976).
D.B.Carlin and W.R.Bennett,Jr., J. Appl. Phys. Vol.49, p.5124 (1978).

TABLE OF CONTENTS

1 - Introduction 1

2 - Mode Locking 3

2.1 Passive Mode Locking 3

2.2 Active Mode Locking 4

2.3 The Mode Locked Argon Ion Laser 5

3 - Second Order Intensity Correlations 10

3.1 The Optical Sampling System 10

3.2 Second Order Intensity Correlation Functions 13

3.3 The Channeltron Photomultiplier Tube and Counting Technique 17

3.4 Relationship Between Mode Locked and CW Correlation Functions 19

3.5 Effects of Broadening Mechanisms on Functional Forms 22

3.6 Validity of the Gaussian Pulse Shape Approximation 25

3.7 Experimental Measurements 27

4 - The Mode Locked, Cavity Dumped Laser 33

4.1 Cavity Dumping 33

4.2 Synchronous Mode Locking ans Cavity Dumping 37

4.3 Output Characteristics 43

4.4 Mode Locked, Cavity Dumped Spectra and Pulse Shapes 44

ACCESSION for
NTIS
DDC
UNANNOUNCED
JUSTIFICATION
DISTRIBUTION/AVAILABILITY CODES
SPECIAL

5 - Technique for the Measurement of Sub-nanosecond Lifetimes 52

5.1 Lifetime Determinations by Gain Measurments 52

5.2 The Argon Ion Laser Lower State Lifetime Experiment 56

5.3 The Sodium Salicylate Lifetime Measurement 63

Appendix I - Acousto-Optical Interactions 70

I.1 Acousto-Optical Mode Locking 70

I.2 Acousto-Optical Cavity Dumping 77

Appendix II - The Laser Sciences Model 254 Laser 83

II.1 Design 83

II.2 Operation 88

II.3 Maintenance 92

References 96

CHAPTER 1 - Introduction

Studies of atomic processes occurring in the sub-nanosecond time domain require excitation mechanisms and detection techniques capable of commensurate temporal resolution. In particular, this laboratory has been interested in lifetime measurements of noble gas ion excited states[1,2]. In this report, techniques for the generation of intense optical pulses and the measurement of time intervals with ~100 psec resolution have been described. In order to demonstrate the utility of these tools, an experiment to measure fast relaxation times was devised. An attempt was made to determine the lifetime of the lower state of the argon ion laser transitions using this method. In order to show the generality of the method, it was applied in a measurement of a fast decay rate in the ultraviolet scintillator sodium salicylate.

The development of mode locking[3-5] has created a convenient method for the generation of optical transients from CW lasers. The argon ion laser is particularly suited to mode locking by acousto-optic diffraction[6] and provides intense pulses of 100 psec duration.

A time interval measurement technique, using second order intensity correlations, has been developed[7]. This method, based on the two-quantum photoelectric effect, has been used to study the shape and duration of the mode locked pulses as a function of the operating conditions

78 10 18 040

of the laser

The incorporation of cavity dumping in the laser system is described in Chapter 4. The mode locked, cavity dumped laser[8] provides a method of further enhancing the peak power of the optical pulses.

Chapter 5 describes the experimental technique for the determination of lifetimes as short as 100 psec. The method was used in an attempt to measure the lifetime of the 4s $^2P_{3/2}$ state of the argon ion. This is the lower state of the strong laser transitions at 4880 Å and 5145 Å and has a lifetime calculated to be 0.36 nsec[9]. A fast relaxation process was observed by this method, and determined to have a lifetime of ≈630 psec.

CHAPTER 2 - Mode Locking

In order to achieve high resolution in time interval studies it is necessary to use optical pulses of extremely short duration. Mode locking is a technique for generating bandwidth limited output pulses from a laser medium. The technique is well-known[3-5] and relies on the synchronization of a periodic loss element to the round trip transit time of light within the laser cavity. All longitudinal modes of that cavity are thereby forced to oscillate with zero phase difference between them. The process is often referred to as "phase locking".

2.1 Passive Mode Locking

The intra-cavity loss is generally effected in one of two ways. For those lasers in which the internally circulating optical power density is high, nonlinear saturable absorbers are often utilized to provide the necessary loss[10]. At low levels of intensity the transmission of light is independent of the incident power density. At higher incident intensities, however, the light depopulates the lower state of the absorber, thereby increasing its transmittance. Thus, light pulses of high intensity are preferentially transmitted over those of lesser intensity.

At the onset of laser oscillation all the longitudinal

modes have randomly distributed phases and the internal electric field consists of chaotic, low power fluctuations. As the internal power density grows, the largest of the pulses begins to bleach the absorber and experiences relatively less loss than do fluctuations of lower intensity. The light circulates within the cavity at frequencies which are separated by

$$\nu_c = \frac{c}{2L} \tag{2.1}$$

where c is the speed of light and L is the distance between the cavity mirrors. With each transit, more bleaching occurs and the most intense pulses are further enhanced. A single pulse eventually dominates the others, capturing most of the energy in the modes.

Organic dyes are effective for these "passive" mode locking applications but usually require incident power densities in excess of 10^6 W/cm^2 for appreciable saturation to occur[11].

2.2 Active Mode Locking

At lower power densities the loss element must be driven by a source other than the laser field itself. The loss must operate at the cavity frequency, ν_c, in "active" mode locking. In addition, the loss must exceed the single pass gain of the amplifying medium. For the argon ion laser used in these studies, acousto-optic

diffraction[12-15] is a convenient way of implementing the required loss (see Appendix I).

2.3 The Mode Locked Argon Ion Laser

The mode locker used in this system is a modulator consisting of a $LiNbO_3$ transducer bonded to a 1" x 1" x ½" block of optical quality fused quartz. A radio frequency sine wave transmitted to the block induces an acoustic standing wave within the quartz. The index of refraction perturbation is proportional to the applied acoustic power density (see equation I.1). The standing wave acts as a grating, perpendicular to the optical axis, which diffracts enough light to extinguish oscillation. Only at those times when the standing wave approaches zero (twice during each rf period), is the optical radiation allowed to propagate through the cavity. If the rf frequency is

$$\nu_{rf} = \tfrac{1}{2}\,\nu_c \tag{2.2}$$

then the mode locking device may be synchronized to the cavity spacing when placed near either end of the cavity. A single pulse which is unattenuated by the mode locker will circulate within the cavity, experiencing further gain with each successive transit.

A Laser Sciences Model 254 argon ion laser tube, described in detail in Appendix II, was employed to

provide the amplifying medium. In normal CW operation, with a 4.3% transmittance output mirror in the cavity, this unit was capable of 900 mW output at either 4880 Å or 5145 Å. The 5145 Å line is most convenient for use in mode locking, having high power but less gain than the transition at 4880 Å. Mode locked operation at the latter wavelength requires that more loss be inserted into the cavity than the acousto-optic modulator is capable of generating as supplied by the manufacturer. The placement of the mode locking element within the cavity introduces substantial losses. The CW output of the laser is decreased to ≈650 mW at 5145 Å with no applied radio frequency power. The mode locked laser system is depicted in Figure 2.1.

The $LiNbO_3$ transducer on the mode locker used had a resonant frequency of 68 MHz, corresponding to a cavity length of 119 cm. There was sufficient response to operate this unit at ±½ MHz from the resonant frequency, so that the radio frequency could be tuned to the cavity length. The fused quartz block has resonant frequencies spaced by ≈250 KHz. Thus, with careful tuning, mode locking could be obtained with ≈⅓ W of applied rf power.

Figure 2.2 is a photograph of a mode locked pulse detected by a Spectra-Physics Model 403 Fast Photodetector. The rise time of the detector is ≈150 psec and the fall time is ≈200 psec for peak optical intensities of 0.5 to

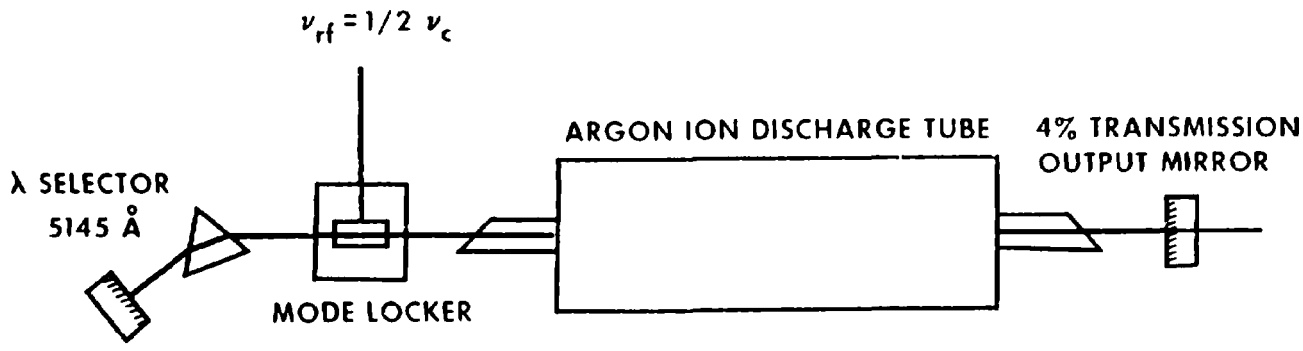

L = CAVITY LENGTH = 110cm

$\nu_c = c/2L = 135\text{MHz}$

FIGURE 2.1 - THE MODE LOCKED ARGON ION LASER

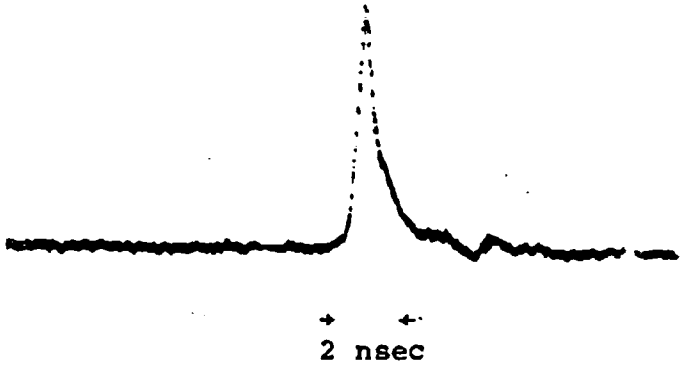

FIGURE 2.2 - MODE LOCKED PULSE

100 mW. Consequently, the laser beam was attenuated with a neutral density 2 filter to avoid damaging the photodiode. The oscilloscope was a Hewlett Packard 1803C/1811A with a 1430 Sampling Head having a rise time of 20 psec. Thus, the apparent pulse duration of ∿500 psec in the photograph is largely due to the photodetector.

When mode locked, the average output power of the laser fell to ≈150 mW. As shown in the following chapter, the duration of the mode locked pulse from the argon ion laser is approximately 100 psec. The repetition rate is twice the radio frequency, or 136 MHz. Thus, the peak power of the pulses is ∿10 W.

CHAPTER 3 - Second Order Intensity Correlations

Studies of optical transient phenomena occurring on sub-nanosecond time scales are severely limited by the response characteristics of conventional photodetectors. Recently, rise times of 50 psec have been reported in Schottky barrier diodes[16]. However, we determined in the conceptual stages of these studies to use an optical sampling technique of far greater inherent resolution. In fact, the temporal resolution of the system described is better than the fastest pulsed light sources known.

3.1 The Optical Sampling System

The optical sampling system used in these experiments is a Michelson interferometer, depicted in Figure 3.1. Incident light is directed into the two arms of the interferometer by a beamsplitter. The variable length arm and the fixed length arm have lengths L_1 and L_2 respectively. The two pulses are recombined by a second beamsplitter. The relative time delay between the pulses is

$$\tau = (L_1 - L_2)/c \qquad (3.1)$$

and the pulses may be swept through one another by varying L_1. The light intensity in each arm may be chosen by selection of the transmission and reflection coefficients of the beamsplitters.

A variable speed DC motor with tachometer feedback

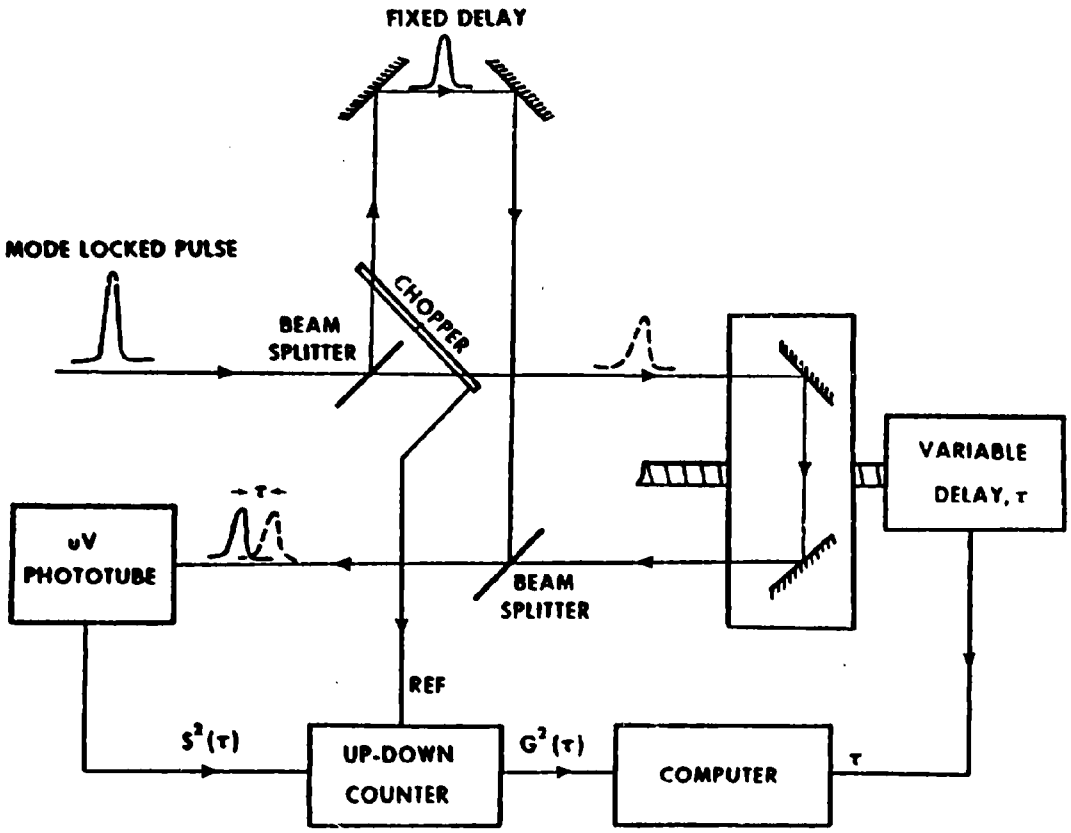

FIGURE 3.1 - THE OPTICAL SAMPLING SYSTEM FOR SECOND ORDER INTENSITY CORRELATIONS

drives a threaded rod through a planetary gear reducer to provide a useful translation speed of ½ cm/min to 2½ cm/sec for the variable length arm of the interferometer. A floating nut couples the threaded rod to the translation stage with neglible transmission of vibration. Also coupled to the threaded rod, through a ten times reducer, is a 50 turn 10 K potentiometer which provides positional data.

Our experiments necessitated that the optical beams be confined to angular deviations of less than 10^{-4} radians for all positions of the translation stage. The stage rides on three linear bearings over two precision ground 1" diameter stainless steel shafts. These shafts are supported at two intermediate points between the end plates to minimize sagging. Careful adjustment of the supports can reduce height deviation due to sagging to 0.001". The interferometer tracks are sufficiently long to allow experiments of up to 6 nsec. In practice, however, it was necessary to keep the length as short as possible for each measurement in order to maintain the angular alignment of the variable length arm beam.

The light is reflected by two pairs of dielectric mirrors, each coated for 99.8% reflectance at 5000 Å for "s" polarized waves at 45° incidence. The mirrors are supported on spring loaded, adjustable mounts to facilitate angular alignment.

3.2 Second Order Intensity Correlation Functions

The utility of two-quantum processes for subnanosecond time resolution has been demonstrated in a number of autocorrelation studies using second harmonic generation[17-21] and two-photon induced fluorescence[22]. We investigated a new technique, based on the two-quantum photoelectric effect, having the promise of simplicity and quantitative accuracy[7].

As presented by Weber and Danielmeyer[23], ambiguities arise in the interpretation of two-quantum experiments without an accurate knowledge of the intensity correlation function. The width of the central peak of this function is approximately the same for normal CW multimode output and mode locked pulses. When many transverse modes are coupled, differences become evident in the details of the functional forms and contrast ratios. With only the TEM_{00} mode oscillating, however, the functional forms become identical and have the same width. The intensity of the correlation signal, however, increases in proportion to the CW signal, as more longitudinal modes are coupled. We have devised a simple and general technique for the determination of the second order intensity correlation function[24]

$$G^2(\tau) = \langle I(t)\,I(t+\tau)\rangle \tag{3.2}$$

based on the two-quantum photoeffect.

By the two-quantum photoeffect we mean the dominant process by which electrons are ejected by a light wave of frequency, ν, for a surface having a work function, W, which satisfies the relationship

$$h\nu < W < 2h\nu. \tag{3.3}$$

There is no first order photoeffect, and the leading non-zero term in a time-dependent perturbation expansion for the electron emission probability is proportional to the square of the total incident optical intensity.

If the electric field of the optical wave in the fixed interferometer arm is denoted by E_1 and that of the variable arm by E_2, where

$$\begin{aligned} E_1 &= E_1(t) \\ E_2 &= E_2(t) \end{aligned} \tag{3.4}$$

then the total field is

$$E = E_1 + E_2. \tag{3.5}$$

Since the optical field is comprised of several frequencies, ω_n, the total field can be written as

$$E = \sum_n \{E_{1n}\, e^{i\omega_n t} + E_{2n}\, e^{i\omega_n (t+\tau)}\} \tag{3.6}$$

where n is the index of the longitudinal modes. For the laser used in these experiments, only the TEM_{00} mode is emitted.

If the two pulses are chosen to be equally intense,

$$E_{1n} = E_{2n} = E_n \tag{3.7}$$

then (3.6) can be expressed as

$$E = 2 \sum_n E_n \, e^{i\omega_n (t+\tau/2)} \cos(\omega_n \tau/2). \tag{3.8}$$

At this point it becomes necessary to distinguish between uncorrelated (CW) light and mode locked (ML) light. For the latter case, the intensity, which is the absolute square of the field, is

$$\begin{aligned} I_{ML} = 4 \sum_{n,m} & E_n E_n^* \, e^{i(\omega_n - \omega_m)(t+\tau/2)} \\ & \cdot \cos(\omega_n \tau/2) \, \cos(\omega_m \tau/2) \end{aligned} \tag{3.9}$$

which can be written as

$$\begin{aligned} I_{ML} = 2 \sum_{n,m} & E_n E_m^* \, e^{i(\omega_n - \omega_m)(t+\tau/2)} \\ & \cdot \{\cos[(\omega_n + \omega_m)\tau/2] + \cos[(\omega_n - \omega_m)\tau/2]\}. \end{aligned} \tag{3.10}$$

The term involving the sum frequency, $\omega_n + \omega_m$, averages to zero more rapidly than does the term involving the difference frequency.

The signal from the two-quantum detector, $S^2(\tau)$, is proportional to the time average of the square of the intensity

$$S^2(\tau) = \langle I_{ML}^2 \rangle \tag{3.11}$$

or,

$$S^2(\tau) = 4 \sum_{\substack{n,m \\ l,k}} \left\{ \left\langle G_{n,l}^{m,k} \, e^{i(\omega_n-\omega_m+\omega_l-\omega_k)(t+\tau/2)} \right\rangle \right. \tag{3.12}$$

$$\left. \cdot \cos\left[(\omega_n-\omega_m)\tau/2\right] \cos\left[(\omega_l-\omega_k)\tau/2\right] \right\}$$

where

$$G_{n,l}^{m,k} = E_n E_m^* E_l E_k^* . \tag{3.13}$$

The time average of the term involving t will vanish unless

$$\omega_n-\omega_m+\omega_l-\omega_k = 0 \tag{3.14}$$

Noting that

$$\omega_n = 2\pi n \nu_c \tag{3.15}$$

then

$$k = n+l-m \tag{3.16}$$

and

$$S_{ML}^2(\tau) = 4 \sum_{n,m,l} G_{n,l}^{m,n+l-m} \cos^2\left[\pi \nu_c \tau (n-m)\right] . \tag{3.17}$$

For CW light,

$$I_{CW} = 4 \sum_n |E_n|^2 \cos^2(\omega_n \tau/2) . \tag{3.18}$$

Therefore,

$$s_{CW}^2(\tau) = 16 \sum_{n,m} |E_n|^2 |E_m|^2 \cdot \cos^2(\omega_n \tau/2) \cos^2(\omega_m \tau/2) \tag{3.19}$$

which can be expressed as

$$S^2_{CW}(\tau) = 4 \sum_{n,m} |E_n|^2 |E_m|^2 \cos^2[\pi\nu_c\tau(n-m)] \qquad (3.20)$$

or

$$S^2_{CW}(\tau) = 4 \sum_{n,m} G^{n,m}_{n,m} \cos^2[\pi\nu_c\tau(n-m)]. \qquad (3.21)$$

In order to derive the two-photon correlation function, $G^2(\tau)$, we note that

$$S^2(\tau) = \langle I^2 \rangle = \langle I_1^2 + 2I_1I_2 + I_2^2 \rangle. \qquad (3.22)$$

Therefore,

$$G^2(\tau) = \langle I_1 I_2 \rangle = [S^2(\tau) - I_1^2 - I_2^2]/2. \qquad (3.23)$$

3.3 The Channeltron Photomultiplier Tube and Counting Technique

The quantity $I_1^2 + I_2^2$ is removed as follows experimentally. After passing through the specially designed chopper, indicated in Figure 3.1, the two optical pulses are recombined and focused on the photosurface of an ultraviolet, solar blind, photomultiplier tube. The particular detector used has a thin film molybdenum photocathode which has a work function of 4.3 eV. Since the laser wavelength is 5145 Å (2.4 eV), this photosurface satisfies the relationship indicated in (3.3). A Channeltron electron multiplier serves as the

amplifier. The single photon sensitivity of the device, determined using the 2537 Å line of a mercury lamp, showed a quantum efficiency of $\sim 10^{-6}$ with saturation occurring at counting rates of 40 KHz. The two-photon process was approximately six orders of magnitude less efficient, as determined by using the CW argon ion laser beam. The Channeltron photomultiplier tube was remarkably free from noise. The dark noise counting rate averaged $\sim$0.2 Hz at room temperature, and only rose to $\sim$1 Hz in the presence of mercury fluorescent room lighting.

The output of the photomultiplier tube is fed through a high speed integral discriminator to a scaler that is switched between add and subtract modes at the command of a reference voltage provided by the chopper. The chopper is a symmetrical two-bladed device, having a LED/photocell reference assembly arranged symmetrically opposite to each of the laser beams. Thus, when a chopper blade is blocking one of the optical paths of the interferometer, the appropriate reference signal is also blocked. The signals from the two photocells are combined by digital logic which gates the add/subtract mode of the scaler. Thus, each chopping cycle is divided into four equal time intervals:

1-counter adds; both beams strike the phototube
2-counter adds; neither beam strikes the phototube
3-counter subtracts; fixed delay beam strikes the phototube alone
4-counter subtracts; variable delay beam strikes the phototube alone.

It is evident that, on the average, this procedure subtracts any residual constant background of the type $\langle I_1 \rangle$ or $\langle I_2 \rangle$ and any double quantum counting terms of the type $\langle I_1^2 \rangle$ or $\langle I_2^2 \rangle$ as well.

3.4 Relationship Between Mode Locked and CW Correlation Functions

Comparison of (3.17) and (3.21) shows the differences in the photomultiplier signal for mode locked and CW light. The expected functional forms are shown in Figure 3.2 together with the correlation function, $G^2(\tau)$, derived by application of (3.23). For this analysis, the light was assumed to have a Gaussian frequency dependence, having a full-width at half-maximum (FWHM) of $2\sqrt{\ln 2}\ \Delta\nu$. For a given number of longitudinal modes, the signal intensities, $S^2(\tau)$, and the correlation functions, $G^2(\tau)$, were numerically computed as a function of time delay, τ. In the example presented in Figure 3.2, nine coupled axial modes were assumed. Figure 3.3 shows the calculated dependence of $G^2_{ML}(0)/G^2_{CW}(0)$ as a function of the number of coupled modes. Thus, the intensity of the mode locked signal grows linearly relative to the CW case for three or more coupled modes. Of course, the concept of mode locking is not valid for only one oscillating longitudinal cavity mode. Additionally, it should be noted that there is no difference either in functional form (both cases having Gaussian shapes) or contrast ratios between $G^2(0)$ and

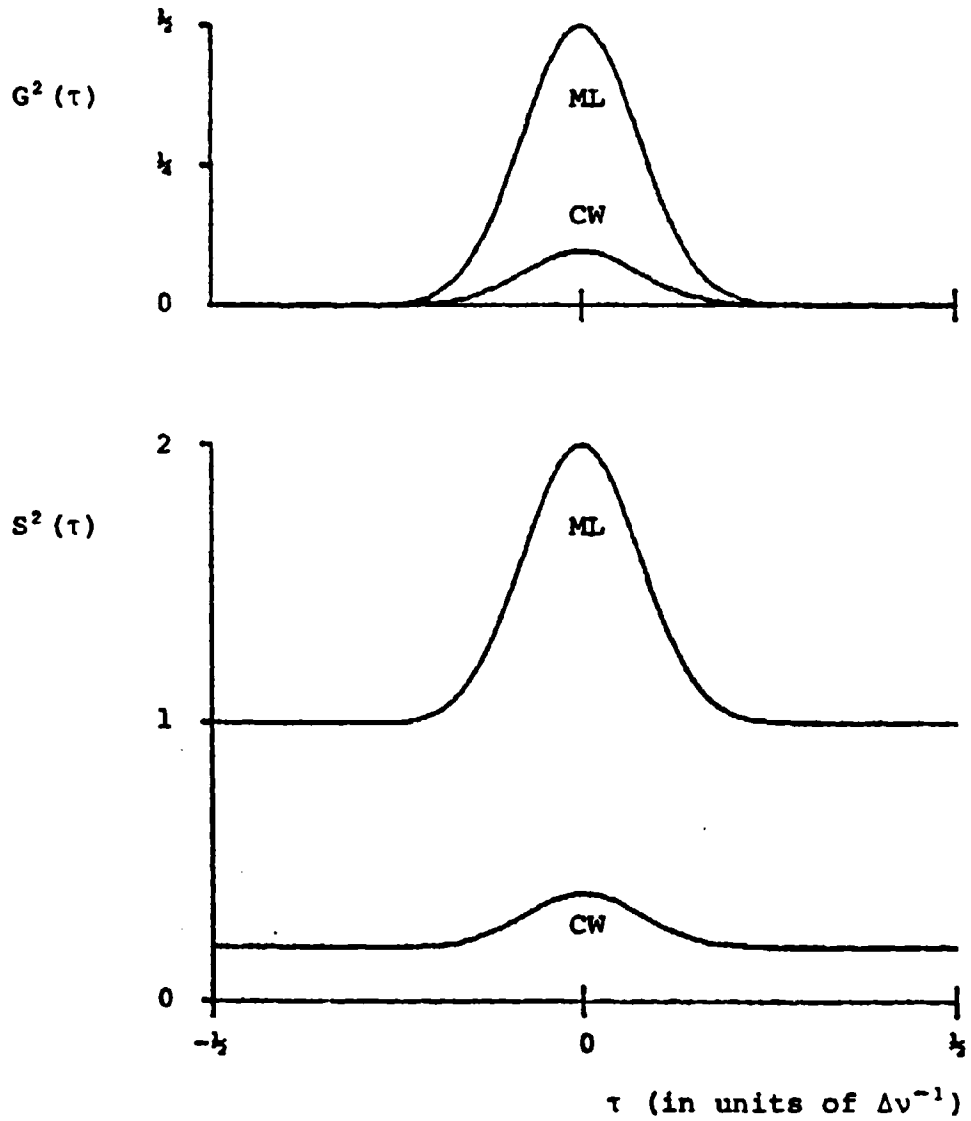

FIGURE 3.2 - INTENSITY CORRELATION FUNCTIONS FOR THE TWO-QUANTUM PHOTOELECTRIC EFFECT

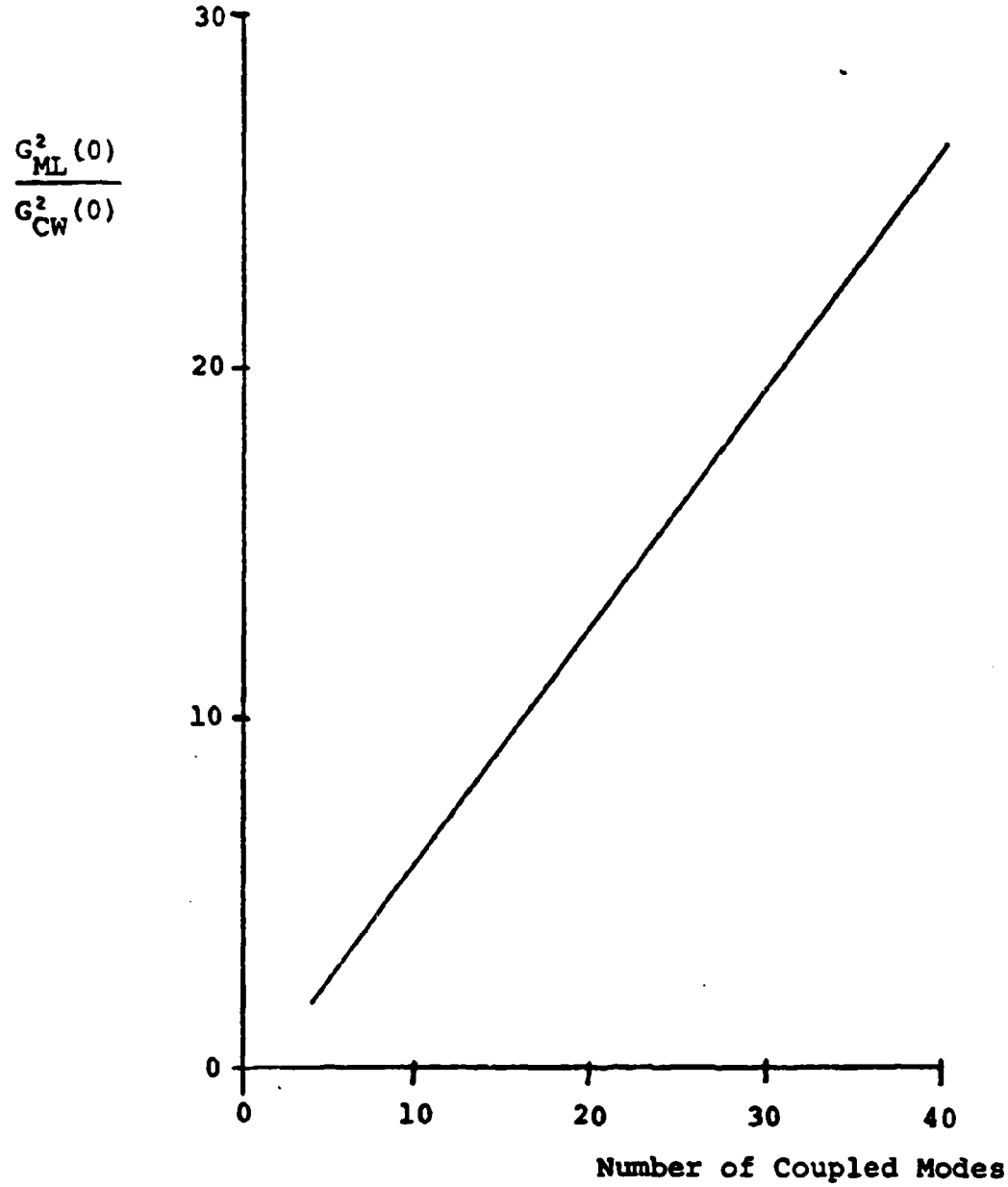

FIGURE 3.3 - STRENGTH OF MODE LOCKED CORRELATION FUNCTION IN PROPORTION TO CW CASE AS A FUNCTION OF THE NUMBER OF COUPLED LONGITUDINAL MODES

$G^2(\tau >> \Delta\nu^{-1})$ as there is in the case of coupled transverse modes[23].

3.5 Effects of Broadening Mechanisms on Functional Forms

In the above analysis a Gaussian frequency dependence was assumed. This is valid for a primarily Doppler broadened transition. However, Lorentz broadening due to collisions will alter the form of the frequency dependence to that of a Voigt profile[25]. In addition, it is of interest to consider the case of a homogeneously broadened laser medium.

Given a frequency distribution, $I(\nu)$, it is possible to calculate the time dependence of the mode locked pulse intensity, $I(t)$. The total electric field is given by the sum of the fields distributed in the modes,

$$E = \sum_n E(\nu_n)\, e^{2\pi i \nu_n t}, \tag{3.24}$$

where

$$E(\nu_n) = [I(\nu_n)]^{\frac{1}{2}}. \tag{3.25}$$

The temporal behavior of the total electric field is obtained by taking the Fourier transform of the above expression;

$$i(t) \propto \sum_{-\infty}^{\infty} [I(\nu_m)]^{\frac{1}{2}}\, e^{2\pi i \nu_m t} \tag{3.26}$$

The intensity of the pulse is the absolute square of the field, or

$$I(t) = |i(t)|^2. \tag{3.27}$$

In Figure 3.4, Lorentzian and Doppler line shapes, having the same full-width at half-maximum (FWHM = $\Delta\nu$), are shown in the left column. I(t) for both cases is presented in the central figures. These functions have strikingly disparate forms and widths. For the Doppler broadened case, the FWHM is

$$T_D = \frac{2\ln 2}{\pi\Delta\nu} \tag{3.28}$$

twice that of the Lorentz broadened case.

It is also possible to obtain analytic expressions for the second order correlation function. Noting that

$$G^2(\tau) \propto \int_{-\infty}^{\infty} I(t)\ I(t+\tau)\ dt, \tag{3.29}$$

we can determine that the second order correlation functions are those shown in the right-hand column of Figure 3.4. In this case, the functional forms and widths of the two distributions differ significantly also. For the Doppler broadened line, the FWHM of the correlation function is

$$T_D = \frac{2\sqrt{2}\ \ln 2}{\pi\Delta\nu} = \frac{1.9605}{\pi\Delta\nu}, \tag{3.30}$$

which is larger than the width of the correlation function in the Lorentzian case. This is

$$T_L = \frac{1.6783}{\pi\Delta\nu}$$

and is determined numerically.

LORENTZIAN LINE SHAPE

$$I(\nu) \propto \frac{1}{1+4\left\{\frac{\nu-\nu_0}{\Delta\nu}\right\}^2} \qquad I(t) \propto e^{-2\pi\Delta\nu|t-t_0|} \qquad G^2(\tau) \propto (2\pi\Delta\nu\tau+1)e^{-2\pi\Delta\nu|\tau|}$$

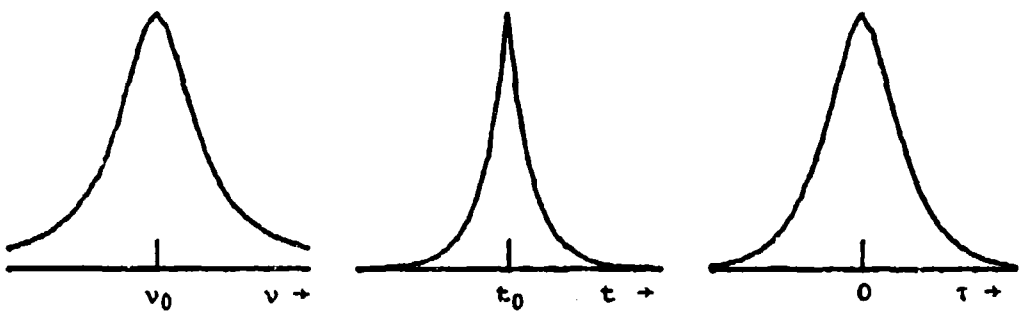

DOPPLER LINE SHAPE

$$I(\nu) \propto e^{-4\ln 2\left\{\frac{\nu-\nu_0}{\Delta\nu}\right\}^2} \qquad I(t) \propto e^{-\frac{\{\pi\Delta\nu(t-t_0)\}^2}{\ln 2}} \qquad G^2(\tau) \propto e^{-\frac{\{\pi\Delta\nu\tau\}^2}{2\ln 2}}$$

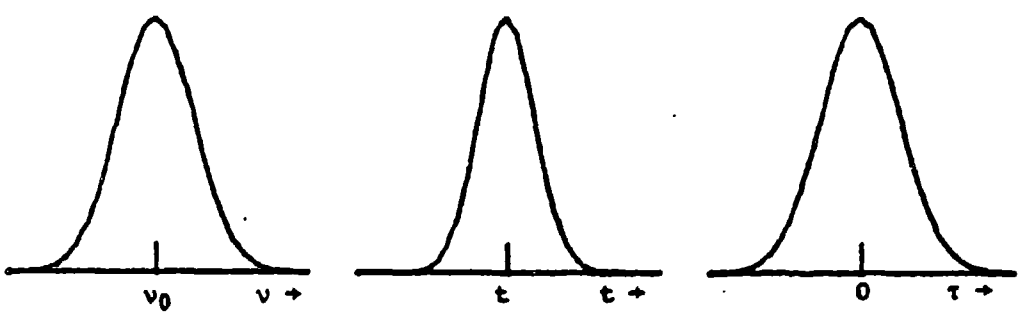

FIGURE 3.4 - FUNCTIONAL FORMS FOR FREQUENCY DISTRIBUTION, $I(\nu)$. TIME DEPENDENCE, $I(t)$, AND CORRELATION FUNCTION, $G^2(\tau)$, FOR MODE LOCKED LASER PULSES

A real gas laser has components of both Lorentz and Doppler broadening due to collisions and the thermal velocities of the excited species. The composite line shape (Voigt profile) is a Doppler distribution of Lorentzians and can be calculated numerically. An example is shown in Figure 3.5 for the argon ion laser system used in the initial mode locking experiments. The cavity spacing, ν_c, is 135 MHz and the loss due to mirror transmission, diffraction, and scattering, is ≈3% per transit. The single pass gain was determined from CW output power measurements, and the Doppler and Lorentz broadening was extrapolated from previous linewidth data by Sze and Bennett[26,27]. The upper curve in Figure 3.5 shows the spectral distribution of the allowed longitudinal modes, computed using the above model for a discharge current of 27 A and an argon pressure of 0.4 torr. The lower curve is the time dependence of the light intensity, obtained by the method outlined in this section.

3.6 Validity of the Gaussian Pulse Shape Approximation

It is now possible to evaluate numerically $G^2(\tau)$ for a Voigt profile line shape using (3.2). Noting, however, that I(t) in Figure 3.5 has a complicated form, there is a strong temptation to approximate the pulse shape with a more convenient function, such as a Lorentzian or a Gaussian. It is clear from Figure 3.4 that the Lorentzian

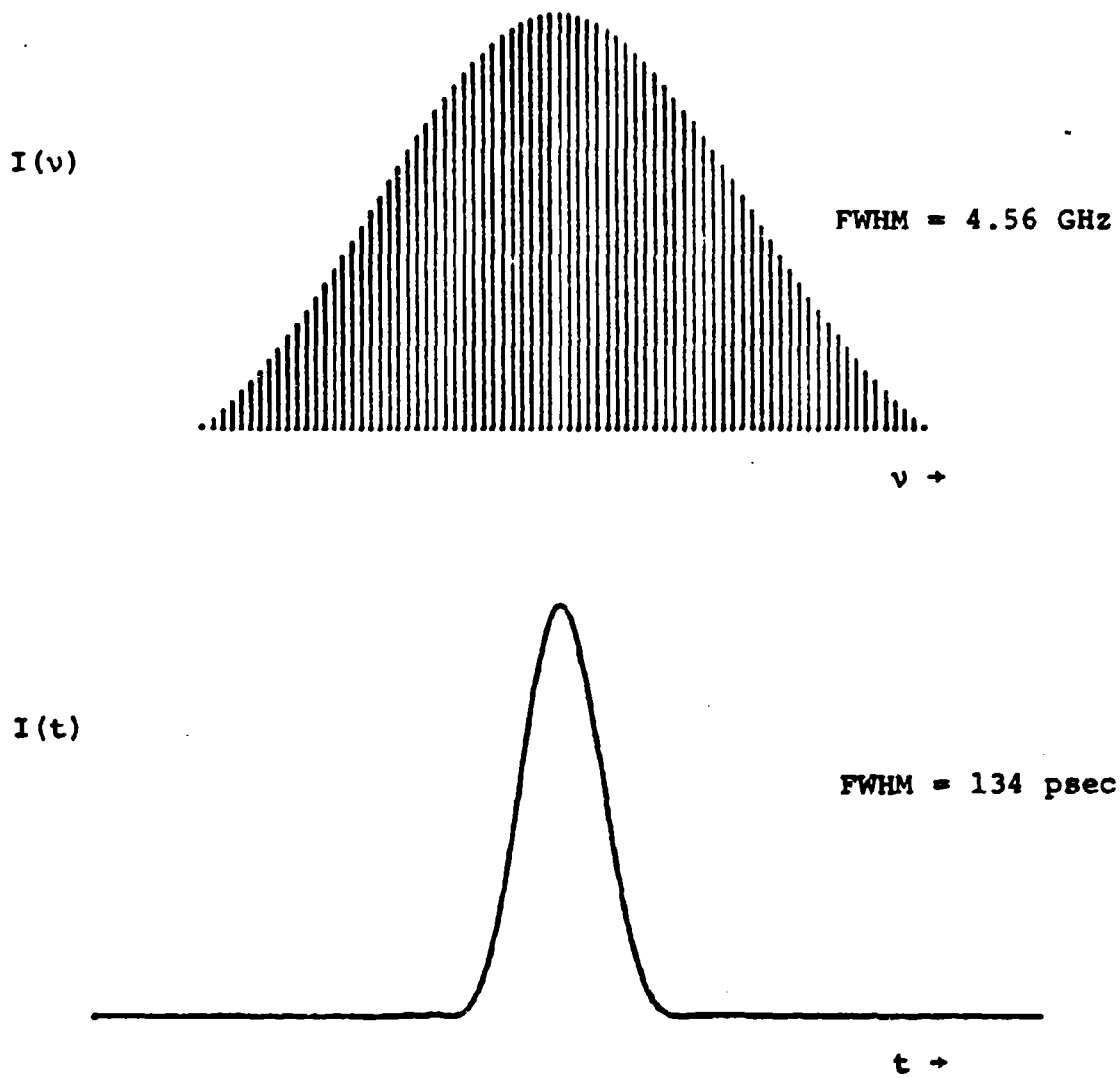

FIGURE 3.5 - FREQUENCY DISTRIBUTION AND TIME DEPENDENCE OF MODE LOCKED ARGON ION LASER PULSE

has little quantitative applicability as an approximation to either $I(t)$ or $G^2(\tau)$. The Gaussian profile, however, appears to be quite suitable in the case of the homogeneously broadened medium. Figure 3.6 shows the validity of the Gaussian approximation to both functions. In the upper figure, the computed Voigt profile $I(t)$ is shown as the dotted curve while the Gaussian least squares fit to a Gaussian functional form is the solid line. The FWHM of the curves are within 3% of each other. The only significant differences occur as the functions approach zero. The Voigt profile generated curve drops off more rapidly, and oscillates with decreasing amplitude as $|t-t_0|$ increases. The lower set of curves are the calculated $G^2(\tau)$ for the Voigt profile (dotted line) and the Gaussian fit (solid line). The approximation is even better in this case. It is important to note that the FWHM of the Gaussian approximation to $G^2(\tau)$ is $\sqrt{2}$ times that of the approximate form of $I(t)$. It is apparent, however, that the Gaussian approximation is a convenient and appropriate device for analyzing mode locked argon ion laser pulses.

3.7 Experimental Measurements

Figure 3.7 is a photograph of the mode spectrum of the mode locked laser, made by passing the laser output into a Spectra Physics Model 470 Optical Spectrum Analyzer. This is a confocal Fabry-Perot interferometer, piezo-

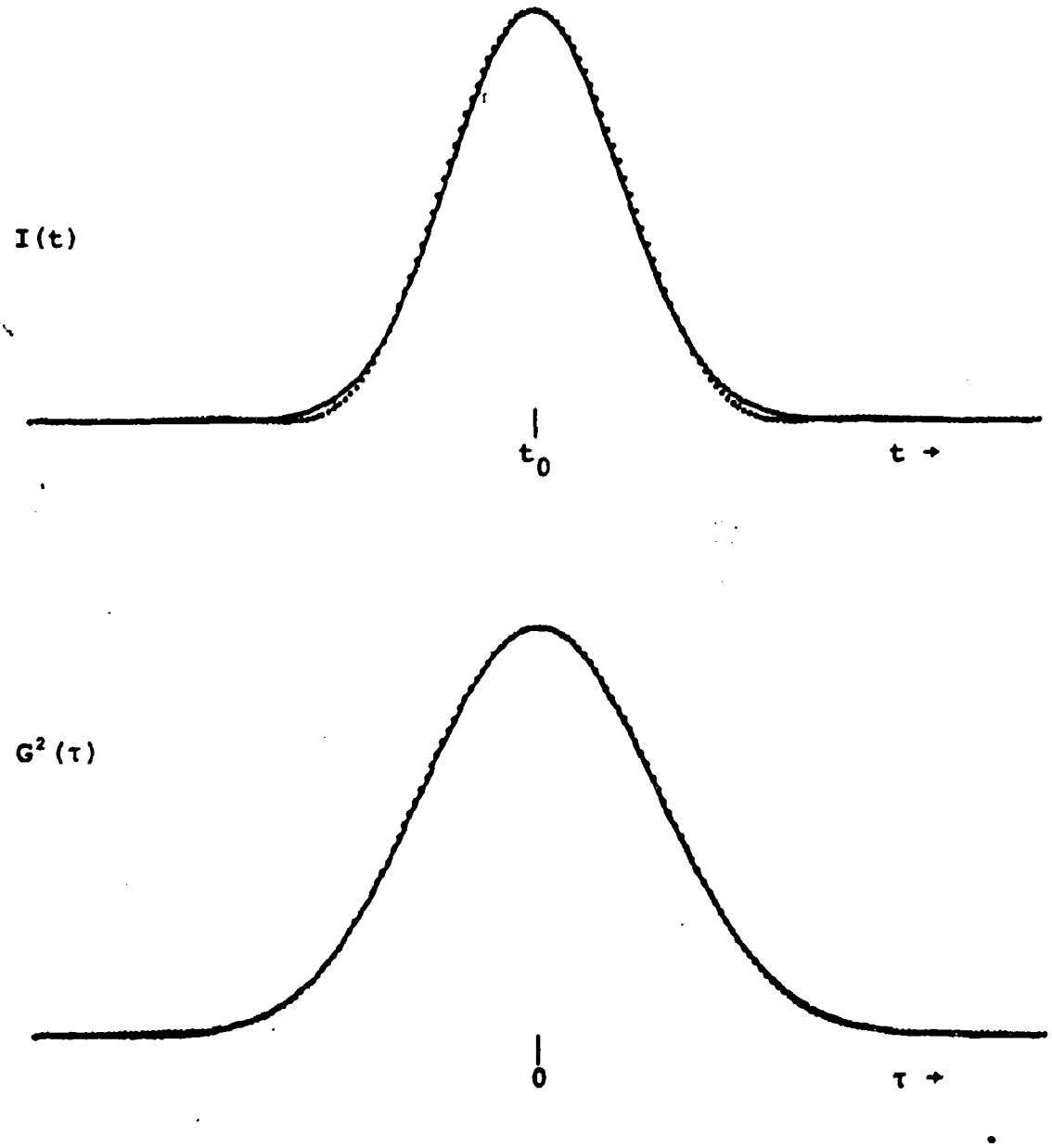

FIGURE 3.6 - GAUSSIAN FUNCTIONAL FORM APPROXIMATIONS TO VOIGT PROFILE GENERATED I(t) AND $G^2(\tau)$

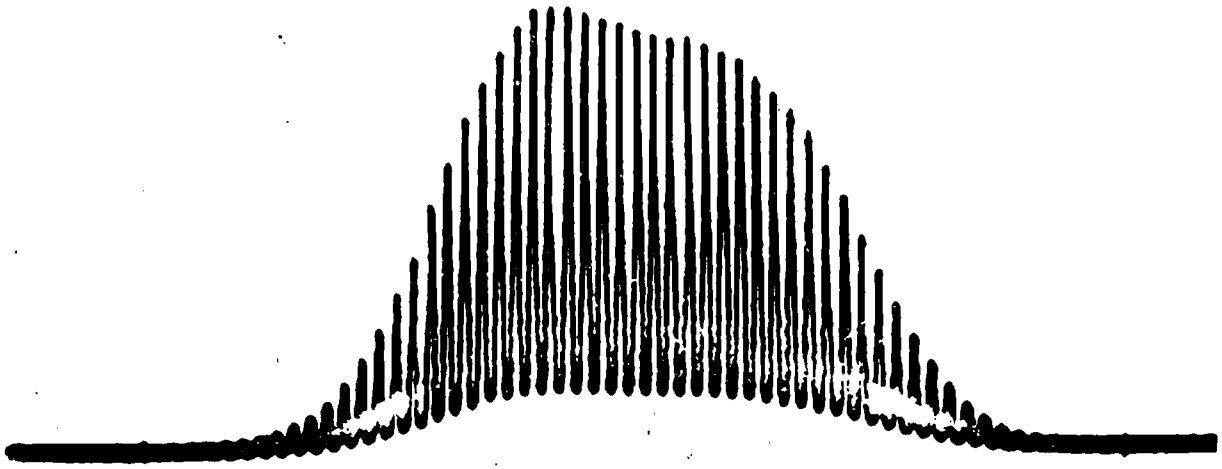

FIGURE 3.7 - THE MODE LOCKED SPECTRUM

electrically scanned, having a free spectral range of 8 GHz and a finesse of 100 at 5000 Å. Note that approximately 42 modes, separated by 135 MHz, are oscillating.

Figure 3.8 is a plot of $G^2(\tau)$ data as a function of time delay. The upper figure shows data for a continuous train of mode locked pulses together with least squares fits to Gaussian (solid curve) and Lorentzian (dotted curve) functional forms. The data was punched in digital form on paper tape by a data acquisition machine. Analysis of five separate runs, made at a discharge current of 30 A, gave an average FWHM response for the original laser pulse of (78.4 ± 3.8) psec. The lower figure shows the two-quantum signal, $S^2(\tau)$, for CW light, plotted in the same relative intensity units as the upper figure. It should be noted that the Lorentzian does not fit the data as well as does the Gaussian, as was predicted.

The applicability of this technique to time interval measurements is demonstrated in Figure 3.9. A 4" thick optical flat was introduced as additional delay into the fixed arm of the interferometer. Both traces are shown in the figure, with the delayed data displayed as the right trace. The least squares fit parameter determining peak location provides a simple method for the measurement of short time delays. Analysis of the data shows that time intervals of ∿100 psec could be consistently measured to within 0.2 psec using the present apparatus.

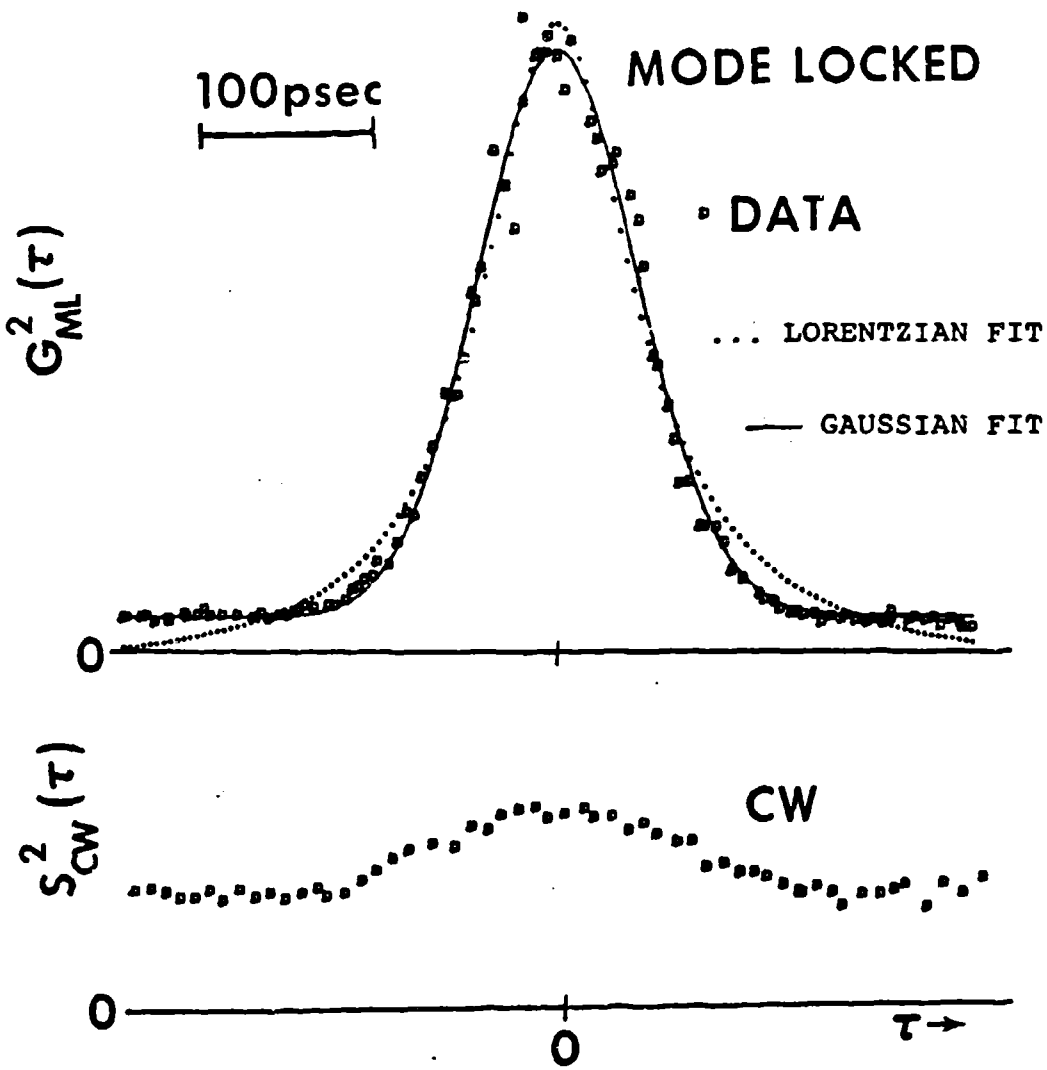

FIGURE 3.8 - SECOND ORDER CORRELATION DATA WITH LEAST SQUARES FITS TO GAUSSIAN AND LORENTZIAN FORMS

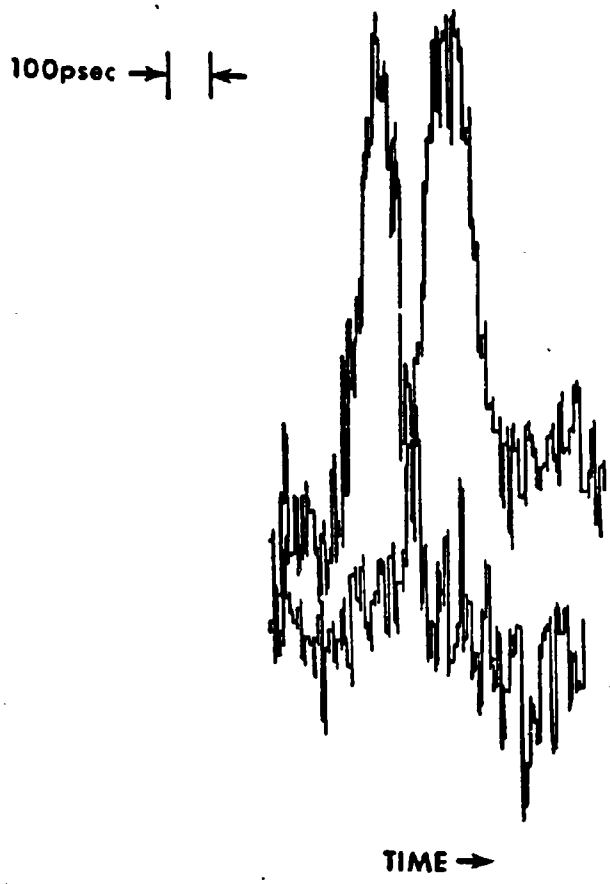

FIGURE 3.9 - SECOND ORDER CORRELATION DATA SHOWING TIME INTERVAL MEASUREMENT TECHNIQUE

CHAPTER 4 - The Mode Locked, Cavity Dumped Laser

4.1 Cavity Dumping

Cavity dumping is a process in which pulses of high peak power are extracted from a laser[28-31]. The power enhancement is effected by increasing both the internal power density and the fraction of light coupled out of the cavity.

In the case of a CW laser, the losses include total dissipative losses, L_d, and output coupling losses, T, per cavity transit[25]. For a laser system in which the light is coupled out of one end of the cavity, T is one-half of the output mirror transmission coefficient. The total loss per pass is

$$L = L_d + T \tag{4.1}$$

and steady-state oscillation occurs when the gain, G, saturates the loss at the oscillation frequency. The removal of excess gain is accomplished through the stimulated emission process and the total laser output power is proportional to the reduction in gain, (G-L). Only a fraction, 2T, is coupled out of the cavity so that the output power may be expressed by

$$P_0 = C(G-L)T/L \tag{4.2}$$

where C is the constant of proportionality. Similarly,

the internally circulating power is

$$P_i = C(G-L)/L. \tag{4.3}$$

For the argon ion laser operating CW at 5145 Å, L_d = 1% and the optimum mirror transmission coefficient ≈ 1%. Thus, the total loss is ≈ 3% per pass. The maximum CW power output is ≈ 1W. Therefore, from (4.2) and (4.3), the internal power is approximately 25 W. In the cavity dumper, the normal 4% output mirror is replaced with a total (99.8%) reflector. The loss drops to ≈1% per pass and the internal power increases threefold.

In order to make use of the internal power enhancement, the cavity dumper redirects the optical beam when output coupling is desired. The device used in this system is shown in Figure 4.1. A traveling wave at a frequency of 470 MHz is transmitted to a fused quartz block through a $LiNbO_3$ transducer. The traveling wave grating, induced by incident rf powers of ≈16 W, is sufficient to deflect ≈50% of the internal beam by an angle of ≈1½° (see Appendix I). One-half of the beam intensity is lost because the CW laser cavity contains running waves traveling in both directions. When used in a mode locked configuration as well, larger fractions of the internal beam may be extracted from the cavity with proper synchronization of the mode locking and cavity dumping processes[32].

For the production of fast cavity dumped output

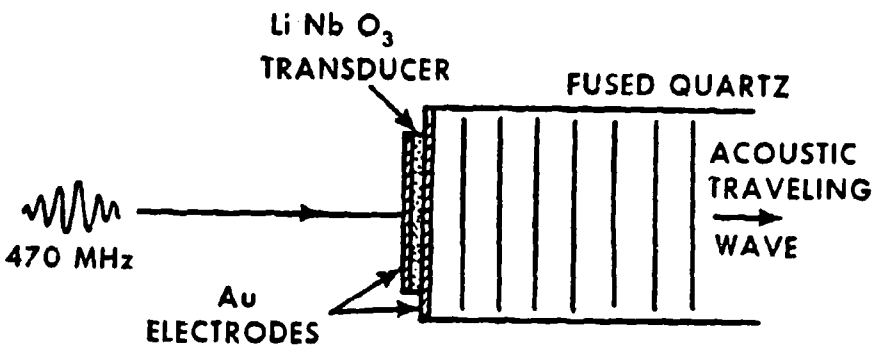

ACOUSTO-OPTIC DEFLECTOR

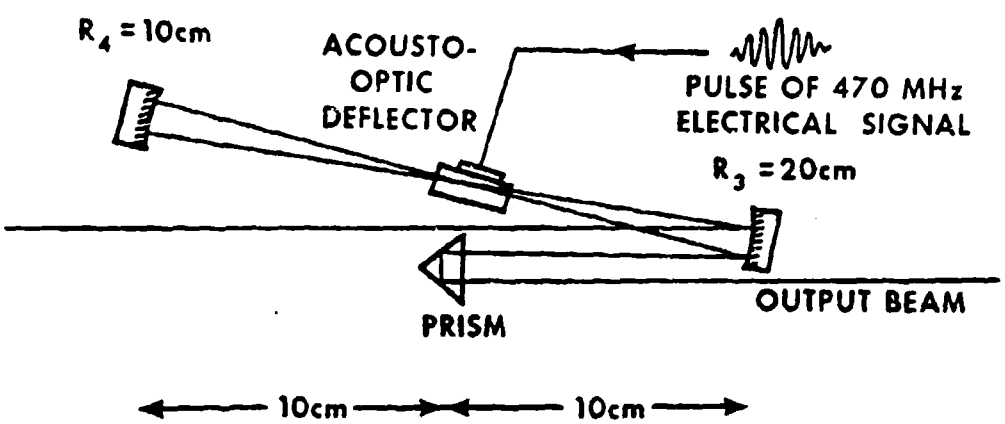

FIGURE 4.1 - THE CAVITY DUMPER

pulses, the transit time for the acoustic wave to cross the optical beam must be minimized. For an optical beam of diameter b, the rise time of the dumping operation will be

$$T_{CD} \sim b/v \tag{4.4}$$

where v is the speed of sound in fused quartz (5968 m/sec). To achieve a narrow beam waist, the light is focused to a diffraction limited spot (≈50 microns) by a concentric cavity formed by R_3 and R_4 in the figure. The internal light beam has a radius of curvature of ≈2 m, twice the cavity length. R_3 is a semicircular total reflector with a radius of curvature of 20 cm. This focuses the light to a point inside the modulator, 10 cm away. The light continues a distance of 10 cm to R_4 having a 10 cm radius of curvature, which reflects it back into the cavity.

When the cavity dumping driver is triggered, the rf traveling wave causes the optical beam to undergo sufficient deflection to displace the optical path by ≈¼ cm at the surface of R_3. Since R_3 has a spherical surface, the reflection of the deflected beam travels parallel to the incoming light for 10 cm, where it is intercepted by a small right angle prism. This, in turn, directs the deflected beam out of the cavity, past R_3. Since the cavity dumper achieves ≈50% output coupling instead of the normal 4%, pulses of 30 W peak power may be extracted.

4.2 Synchronous Mode Locking and Cavity Dumping[8]

It is natural to consider applying cavity dumping, with its thirtyfold peak power amplification, to the mode locked laser described in Chapter 2. Typical output characteristics for the mode locked system are pulse durations of 100 psec, repetition rates of 135 MHz, and measured average power levels of 100 mW. It is reasonable to expect that the ≈7 W peak power mode locked pulses will be enhanced to ≈200 W peak power using cavity dumping. We, therefore, sought to develop a flexible method for extracting individual mode locked pulses using cavity dumping.

Unfortunately, the available optical modulators and the discharge tube had physical sizes which were not compatible with the 110 cm cavity length required by our mode locker. The discharge tube is ≈75 cm long, and the mode locker and wavelength selector require an additional 15 cm. The cavity dumper uses more than 40 cm of cavity length. Clearly, a solution other than a straight-forward assembly of the components was needed.

As long as the fundamental acoustic resonance of the mode locking transducer is low enough, the cavity can be lengthened to include all of the elements of the system. Thus, if the required overall length is L, a harmonic, n, of the fundamental transducer resonance, f_0, may be chosen

such that

$$nf_0 = \frac{c}{4L}. \tag{4.5}$$

In the case of the transducer used in this mode locker, shown in Figure 4.2, n is odd so that the standing wave is always zero at the far end of the fused quartz block. In this particular case, we found that the transducer was being driven at the third harmonic of its fundamental resonance as supplied by Spectra Physics. We were able, therefore, to lengthen the cavity to ≈330 cm, more than adequate to accommodate all the elements of the system.

For this extreme cavity length and small discharge tube bore diameter, however, diffraction losses play an important role. Figure 4.3 shows the diffraction losses in the TEM_{00} mode for a confocal cavity as a function of the Fresnel number $a^2/L\lambda$, where a is the radius of the limiting aperture within the cavity projected onto the curved mirror[33,34]. In this case, the cavity length is 333 cm and the bore diameter is 2½ mm. If the laser tube is placed optimally (as near to the mode locker and wavelength selector as possible) then a=1.36 mm. The Fresnel number is, then, 0.54. As the figure shows, this leads to diffraction losses of ≈7% which is a prohibitive amount.

This condition can be avoided by folding the cavity as shown in Figure 4.4. The wavelength selector and mode locker are located at the flat mirror end of the cavity. The folding mirror chosen has a radius of curvature of

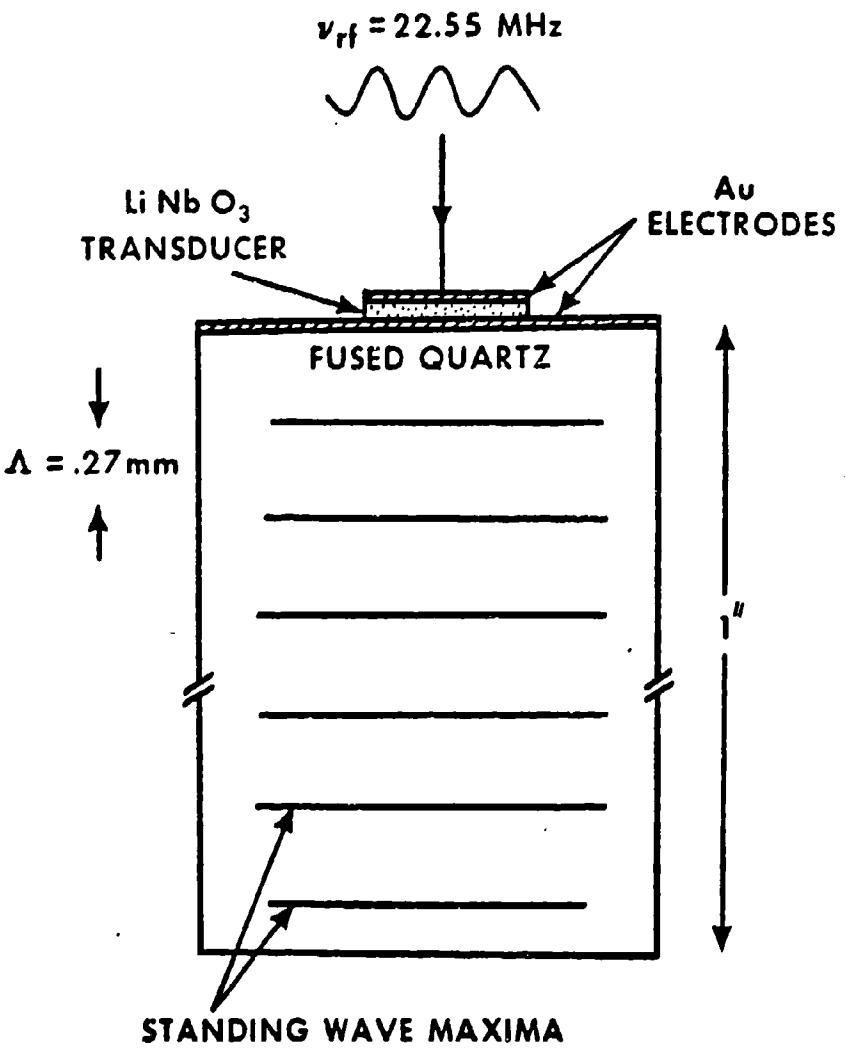

FIGURE 4.2 - MODE LOCKER USED IN THE CAVITY DUMPED LASER

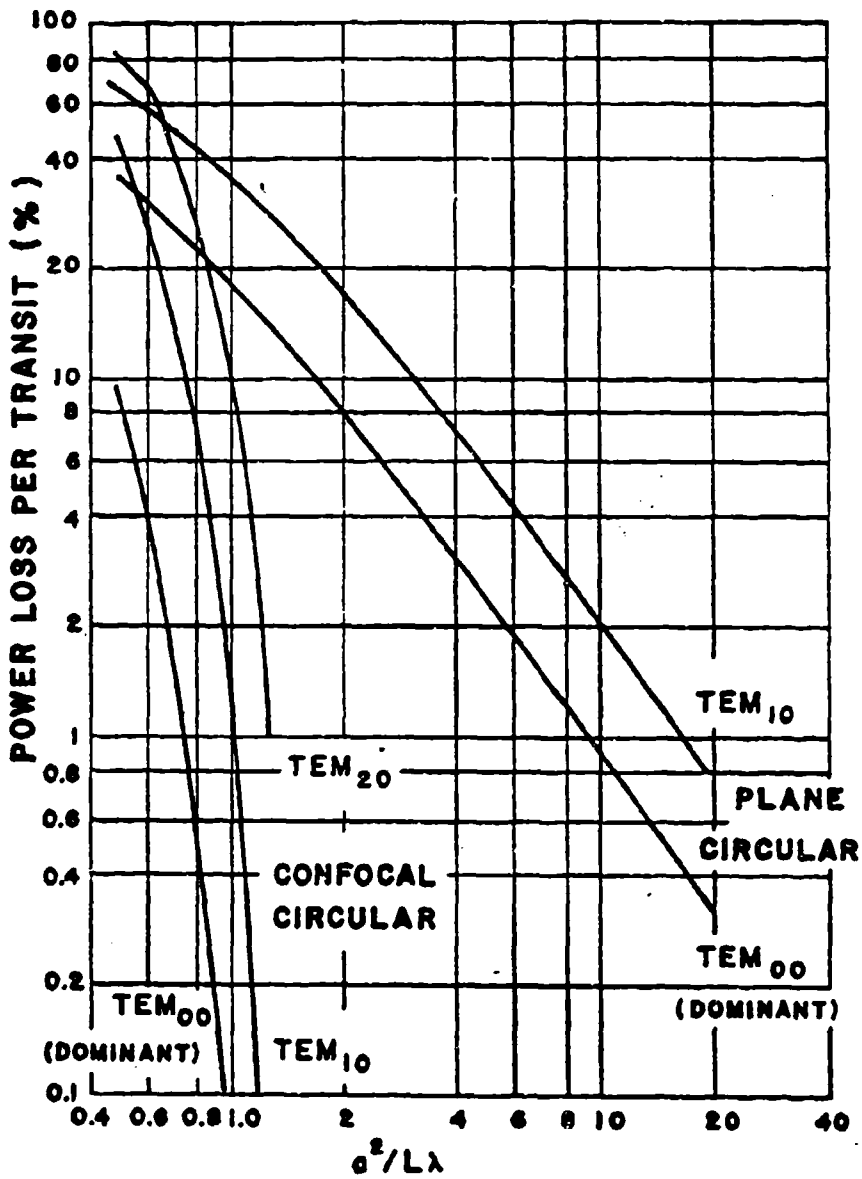

FIGURE 4.3 - DIFFRACTION LOSSES AS A FUNCTION OF THE FRESNEL NUMBER, $a^2/L\lambda$

[From Bennett[25]]

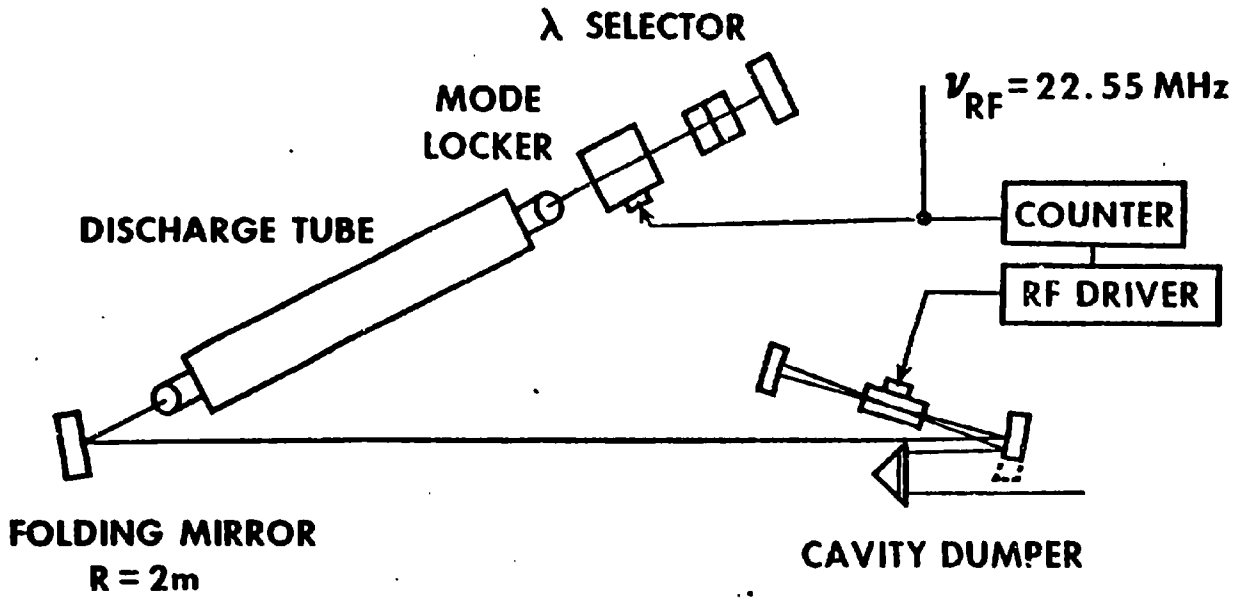

FIGURE 4.4 - THE MODE LOCKED, CAVITY DUMPED LASER

2 m and would result in a conventional confocal mode with a Fresnel number of 1.43. By offsetting the angular alignment of the folding mirror as shown, the original confocal cavity modes are effectively coupled into a second tandem confocal equivalent resonator with similar optical properties. Consequently, a wave launched at the flat mirror end in a TEM_{00} mode will be matched into a spherical surface of constant phase with a 2 m radius of curvature when it arrives at the first mirror (R_3) of the cavity dumper. Thus, we have achieved an optical path of 3.3 m within the folded cavity with neglible increase in diffraction losses over the original 1.1 m cavity.

Of course, the rf oscillator and amplifier originally supplied to drive the mode locker are no longer useful. The extended cavity requires that the mode locker be driven at 22.5 MHz. A Hewlett-Packard Model 608D radio frequency oscillator now provides this frequency. An ENI Model 300L amplifier provides up to 3 W of rf power for mode locking. As the oscillator has a tendency to drift in frequency for several hours following turn on, it was allowed to stabilize in frequency before mode locking could be effected.

Fast digital logic is used to count mode locked rf periods and trigger the cavity dumping driving electronics. The mode locked pulses circulating within the cavity require approximately 300 nsec (∿30 transits of the gain

medium) to saturate the amplification mechanism. Dumping at repetition rates faster than 3 MHz does not allow the pulse sufficient time to build up to maximum power. Slower output coupling does not increase the peak power, but diminishes the average power. A gating delay allows for synchronization of the mode locked peak within the cavity dumped envelope. The rise time of the cavity dumper and the round trip transit time for light within the cavity are both ≈20 nsec. Thus, with the cavity dumper running wave set for minimum duration, a single mode locked pulse can be extracted. This would not have been possible using a shorter cavity and these same acousto-optic modulators. An increase in the duration of the 470 MHz running wave permits multiple pulse operation (see Figure 4.5).

4.3 Output Characteristics

Average power measurements were made with the system operating at repetition rates of 3 MHz. Under conditions of high gain (discharge currents of 25-30 A), the average power was ≈45 mW. For a pulse duration of ≈150 psec, this indicates that ∿100 W peak power pulses are generated by this system.

4.4 Mode Locked, Cavity Dumped Spectra and Pulse Shapes

A knowledge of the shape and duration of the mode

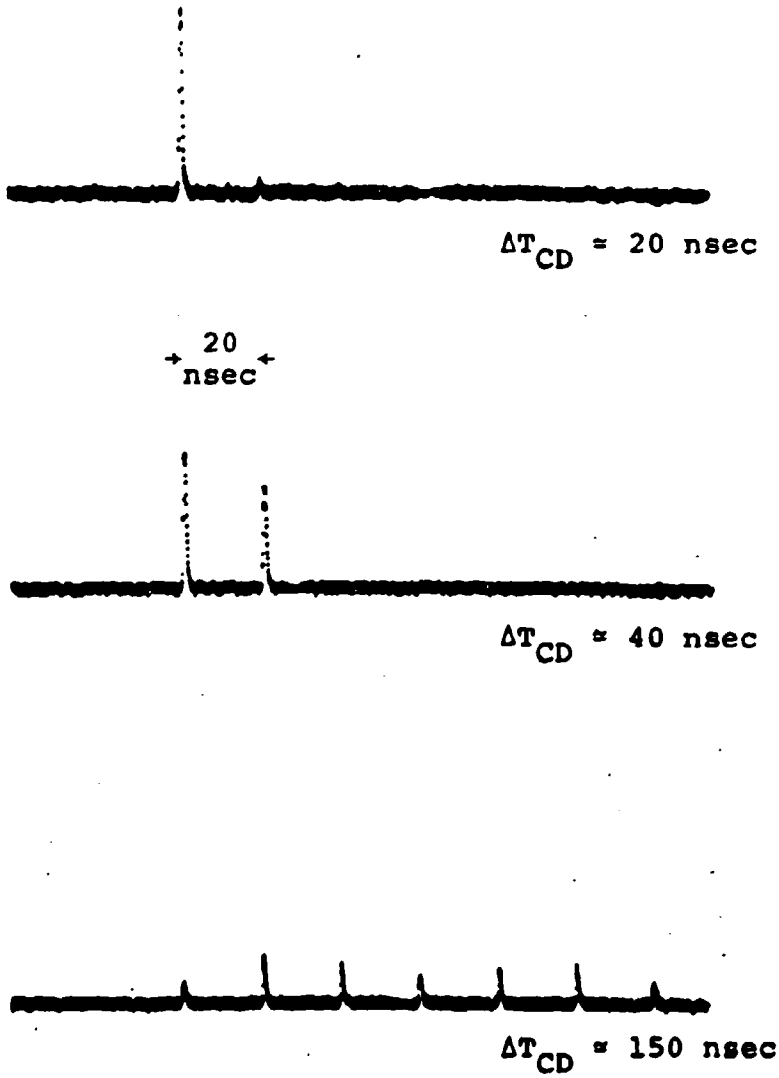

FIGURE 4.5 - MULTIPLE PULSE OPERATION AS A FUNCTION OF CAVITY DUMPER RF DURATION, ΔT_{CD}

locked, cavity dumped pulses is useful in the analysis of studies making use of these pulses. The pulse shape may be predicted from the same model used in generating Figure 3.5, modified for the operating conditions appropriate to the mode locked, cavity dumped sytem. The losses in this system are expected to be somewhat less than those in the mode locked laser as the output mirror transmittance is now zero. However, the modulator introduces ∿1% loss. Thus, total losses of 2% per transit are used in the calculations.

The argon laser required fewer refillings, and operated at higher powers after a burn-in time of ∿30 minutes, when the filling pressure was increased to 0.9 torr. The increased pressure causes slightly greater Lorentz widths and smaller Doppler widths than the pressure used in calculating the mode locked model[26]. The computer-generated spectral distributions and time dependent intensities are shown in Figures 4.6 a-d. All maxima have been normalized to the same value, as the intention is to show shape and width variations. The discharge currents in the four calculations are: a) 15 A, b) 20 A, c) 25 A, and d) 30 A. The mode spacing is only 45 MHz for the 3.3 m cavity. This causes the mode structure, visible in Figure 3.5, to be obliterated in the present case.

The spectral bandwidths and pulse durations were experimentally determined using Fabry-Perot interferometry

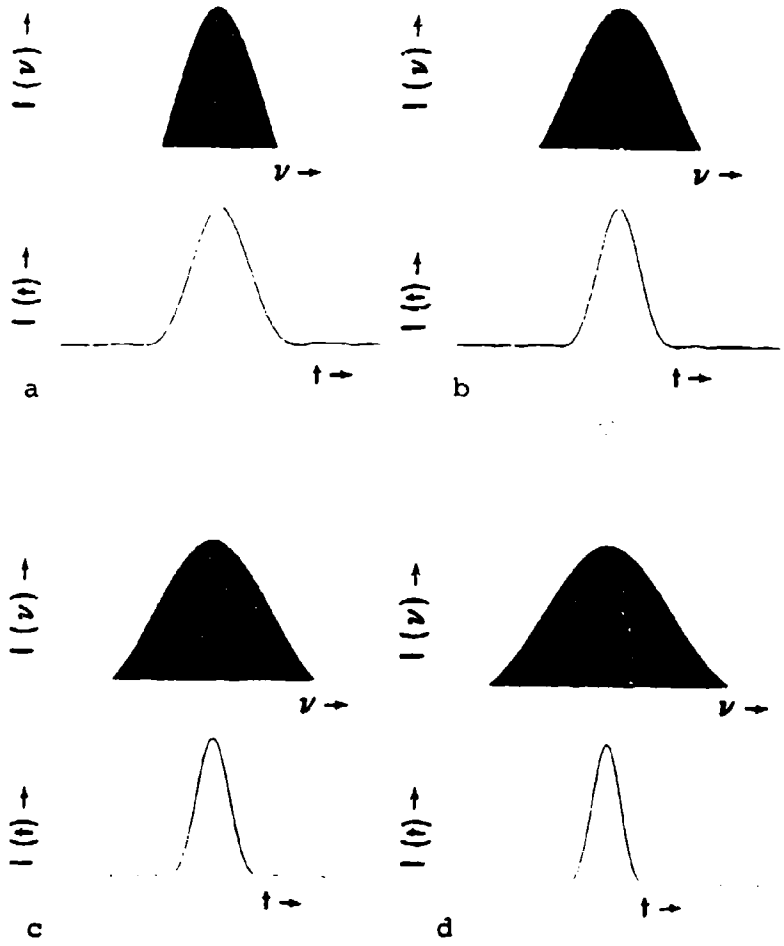

FIGURE 4.6 - SPECTRAL DISTRIBUTIONS AND TIME DEPENDENCE OF MODE LOCKED, CAVITY DUMPED PULSES: a) 15 A, b) 20 A, c) 25 A, d) 30 A

and second order intensity correlation measurements. In the mode locked, cavity dumped system, the close spacing of the longitudinal cavity modes requires Fabry-Perot mirrors having reflectances of >99.2% in order to resolve the mode structure, as in Figure 3.7. Such optics were unavailable. However, the convenience of having the mode structure as a frequency reference is not necessary in order to determine the FWHM of the spectrum. Instead, the free spectral range of the interferometer was used to provide the frequency reference.

A pressure scanned Fabry-Perot was aligned so that part of the optical beam passed through it to a photomultiplier behind a 1 mm aperture. The beam was attenuated with neutral density filters to prevent saturation of the phototube. The pressure scanning was effected by venting high pressure (~150 atmospheres) N_2 gas into the interferometer chamber through a small leak to provide linear flow. The Fabry-Perot had a free spectral range of 15 GHz and the pressure was allowed to scan 5-7 free spectral ranges. The full-width at half-maximum of each transmission maximum was determined and related to the distance between adjacent maxima on a strip chart record of the data. Figure 4.7 is a sample of the interferometer data, with two maxima shown. The results of several analyses, for data taken at varying discharge currents, is shown in Figure 4.8. The predicted bandwidths for

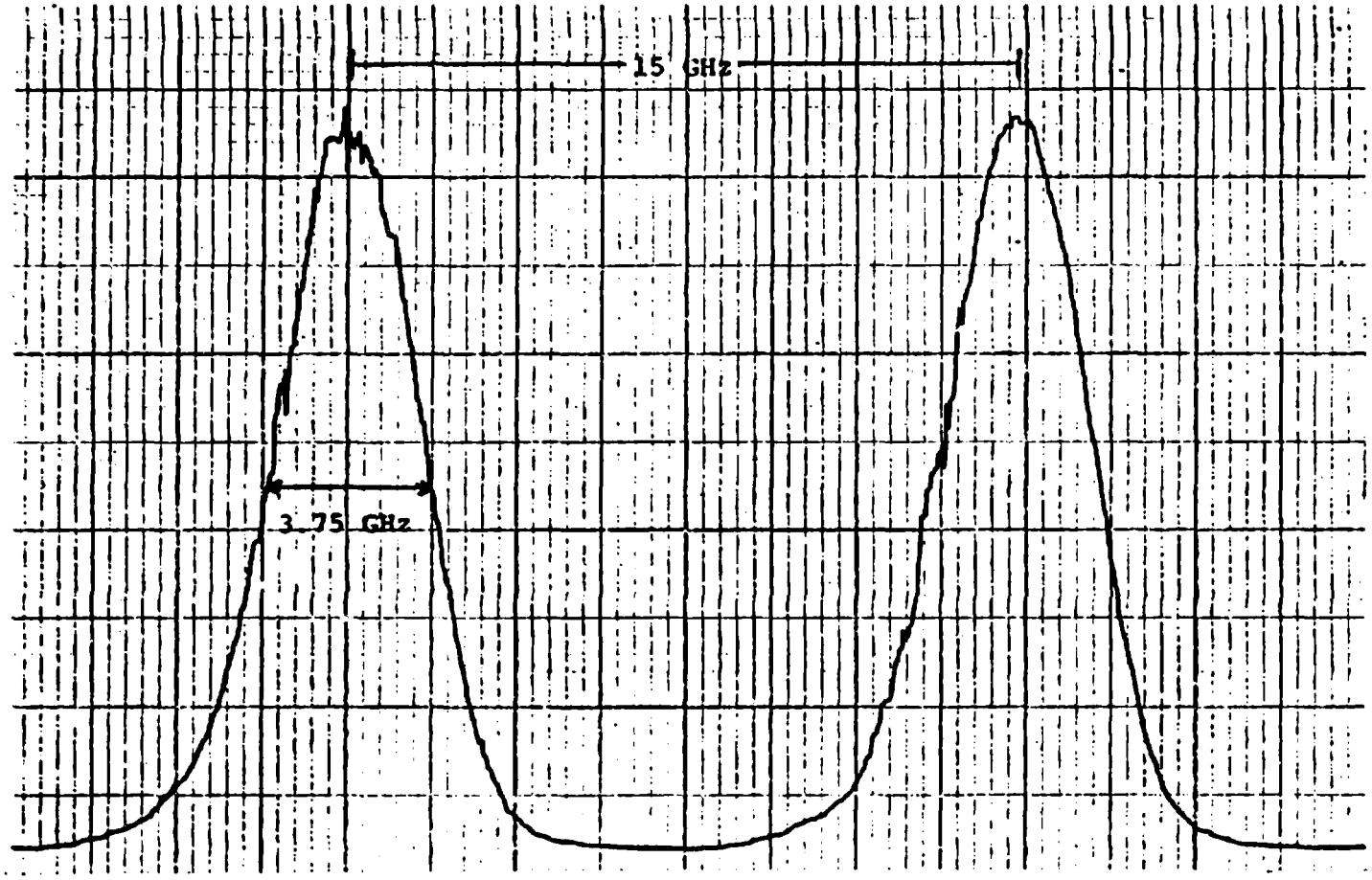

FIGURE 4.7 - FABRY-PEROT INTERFEROMETER SCAN OF THE SPECTRUM OF THE MODE LOCKED, CAVITY DUMPED ARGON ION LASER (PRESSURE = 0.95 TORR, DISCHARGE CURRENT = 18 A)

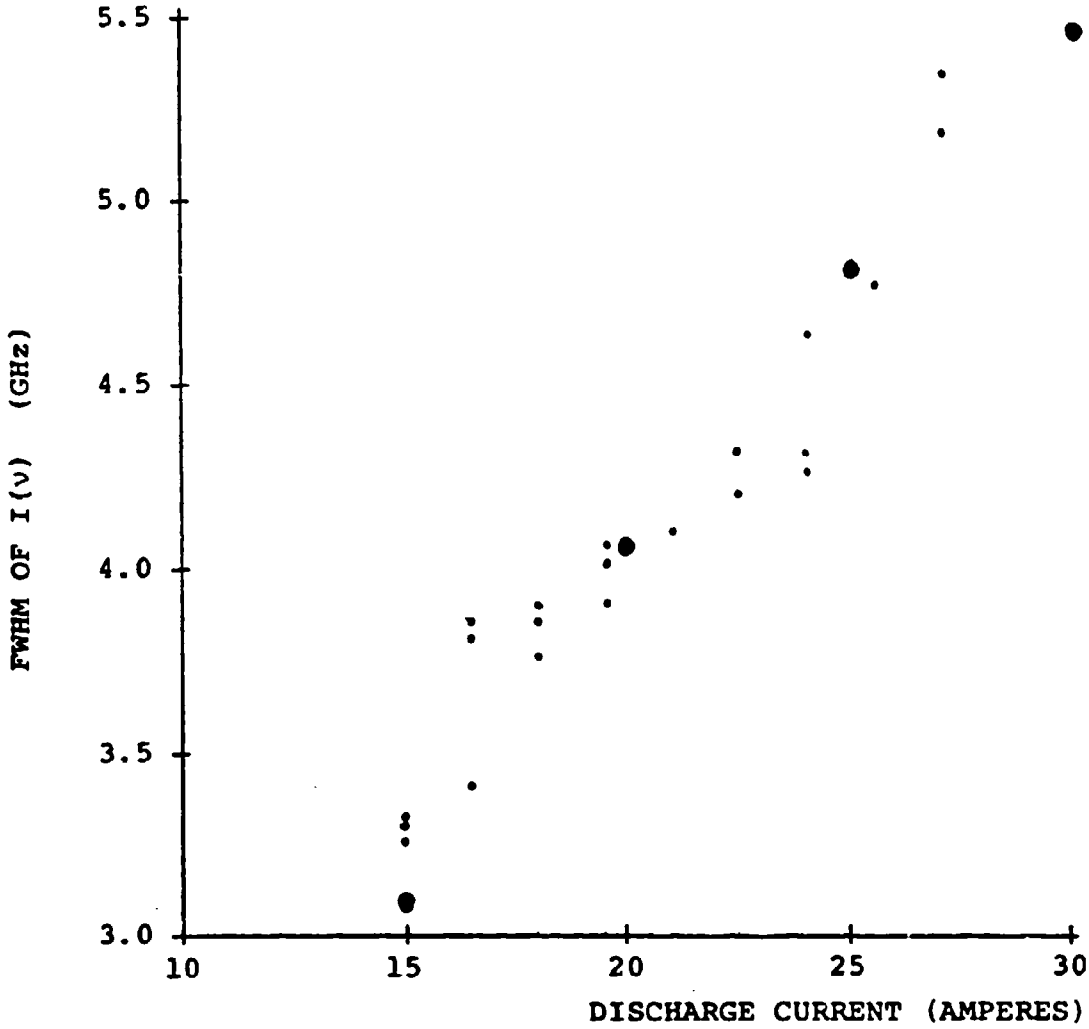

FIGURE 4.8 -SPECTRAL WIDTH AS A FUNCTION OF CURRENT IN THE MODE LOCKED, CAVITY DUMPED LASER (ARGON PRESSURE = 0.95 TORR)

currents of 15, 20, 25, and 30 A from the computer analysis are included as the larger points in the figure.

The pulse durations indicated in Figure 4.6 are plotted in Figure 4.9 as a function of discharge current together with two-quantum correlation data. The model (larger points) predicts slightly shorter pulses than were generated experimentally. Imperfect mode locking[35] results when ν_{rf} drifts more than ≈500 Hz from $\frac{1}{2}\nu_c$. Thus, the results shown in Figure 4.9 are not surprising.

The product of the spectral bandwidth and pulse duration FWHM range from 0.678 at 15 A to 0.606 at 30 A as determined using the computer model. The experimental values for this product are in the 0.6 to 0.9 range. For ideal mode locked pulses from a purely Doppler broadened medium, having no cavity losses, the product of bandwidth and duration is $2\sqrt{\ln 2}/\pi = 0.44$. Thus, it is possible to estimate either the gain bandwidth of the laser medium or the duration of the mode locked pulse generated by that laser from a knowledge of the other quantity.

At higher currents there is only a weak dependence of pulse duration on current. Durations of ≈150 psec are obtainable at 24 A. At 30 A, this is only decreased to 125 psec. Therefore, if ultimate temporal resolution is not required, it is prudent to operate the laser at low current levels in order to prolong its life.

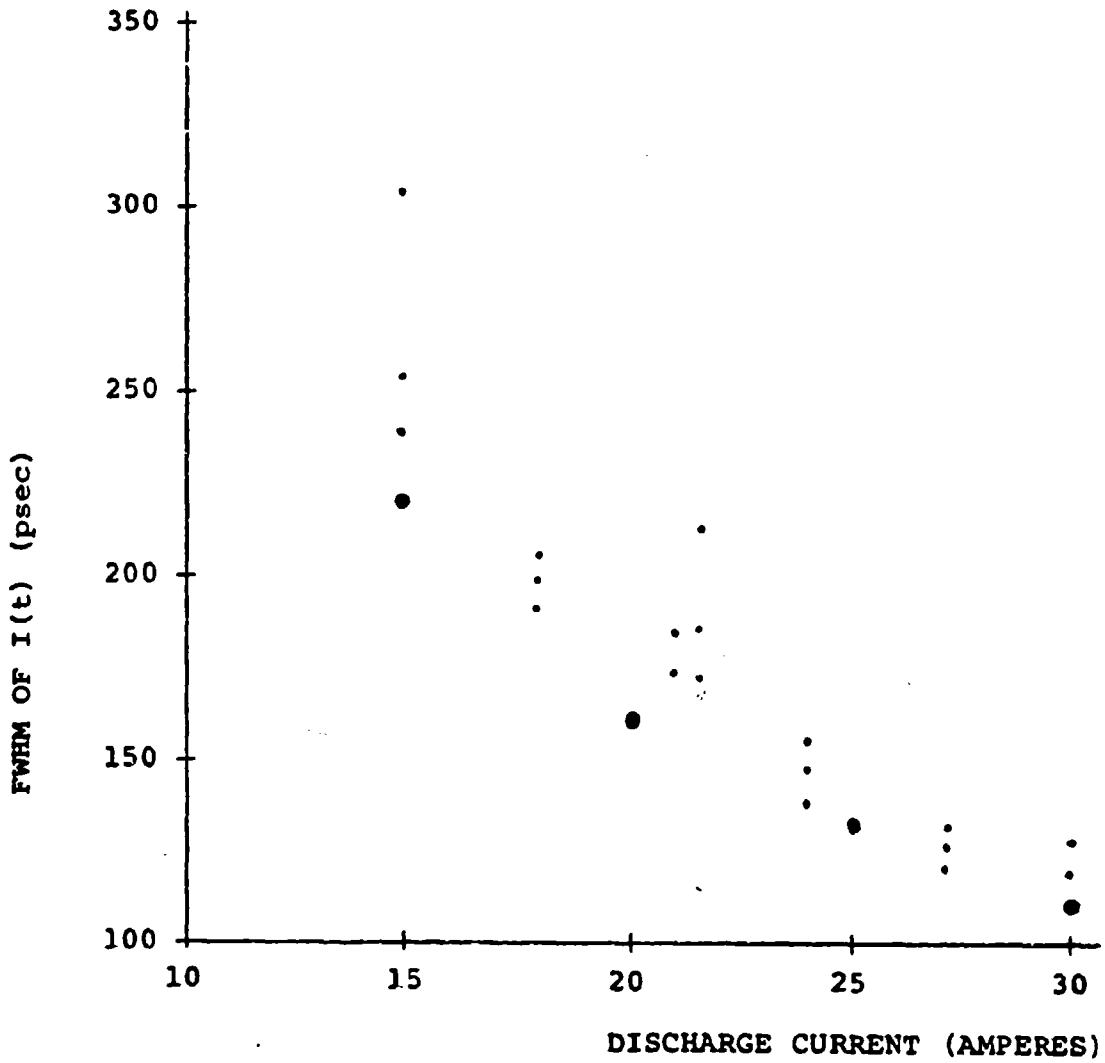

FIGURE 4.9 - PULSE DURATION AS A FUNCTION OF CURRENT IN THE MODE LOCKED, CAVITY DUMPED LASER (ARGON PRESSURE = 0.95 TORR)

CHAPTER 5 - Technique for the Measurement of Sub-nanosecond Lifetimes

Many atomic and molecular relaxation processes occur at rates which are inaccessible to conventional electronic measurement techniques. We have developed a method, using mode locked laser pulses and the optical sampling system, which permits the measurement of lifetimes as short as 100 psec.

The intense laser pulses can be used to perturb the populations of the upper and lower states of a resonant transition in the investigation sample. The subsequent relaxations of the population densities of these states can be used to determine their effective lifetimes. If the mode locked pulses are sufficiently intense, optical sampling of the time-dependent gain or absorption of the medium at the laser wavelength can be effected using the Michelson interferometer.

5.1 Lifetime Determinations by Gain Measurements

In the evolution of the populations of the system considered, the lower and upper states have relaxation rates A_1 and A_2 respectively. The time-dependent population density of the upper states is

$$n_2(t) = n_2 e^{-A_2 t} \tag{5.1}$$

where n_2 is the difference between the initial and perturbed

population densities. The lower state will include a contribution due to radiative cascade from the upper state[1]

$$n_1(t) = [n_1 - \frac{A_{21}n_2}{A_1 - A_2}]e^{-A_1 t} - [\frac{A_2 n_2}{A_1 - A_2}]e^{-A_2 t} \qquad (5.2)$$

where A_{21} is the transition probability connecting the two states and n_1 is the quantity corresponding to n_2 for the lower state. The population difference is, then,

$$n_2(t) - n_1(t) = [1 - \frac{A_{21}}{A_1 - A_2}]\ n_2 e^{-A_2 t} - [n_1 - \frac{A_{21}n_2}{A_1 - A_2}]\ e^{-A_1 t} \qquad (5.3)$$

which may be simplified to

$$n_2(t) - n_1(t) = N_2 e^{-A_2 t} - N_1 e^{-A_1 t}. \qquad (5.4)$$

At resonance, the small signal gain of a running wave is[25]

$$G(t) = \frac{1}{I}\frac{\partial I}{\partial z} = [n_2(t) - n_1(t)]\ \frac{\lambda^2 A_{21}}{2\pi(A_1 - A_2)}\ . \qquad (5.5)$$

Thus, the change in intensity of a weak beam which probes the perturbed system at time delay, τ, is

$$\Delta I(\tau) = \Delta I_0 \exp\{B_2 e^{-A_2 t} - B_1 e^{-A_1 t}\} \qquad (5.6)$$

where I_0 is the maximum intensity perturbation and B_1 and B_2 incorporate the constants in (5.3) and (5.5).

Figure 5.1 illustrates the experimental technique for lifetime measurements using optical sampling. A strong pulse from the fixed path of the interferometer perturbs

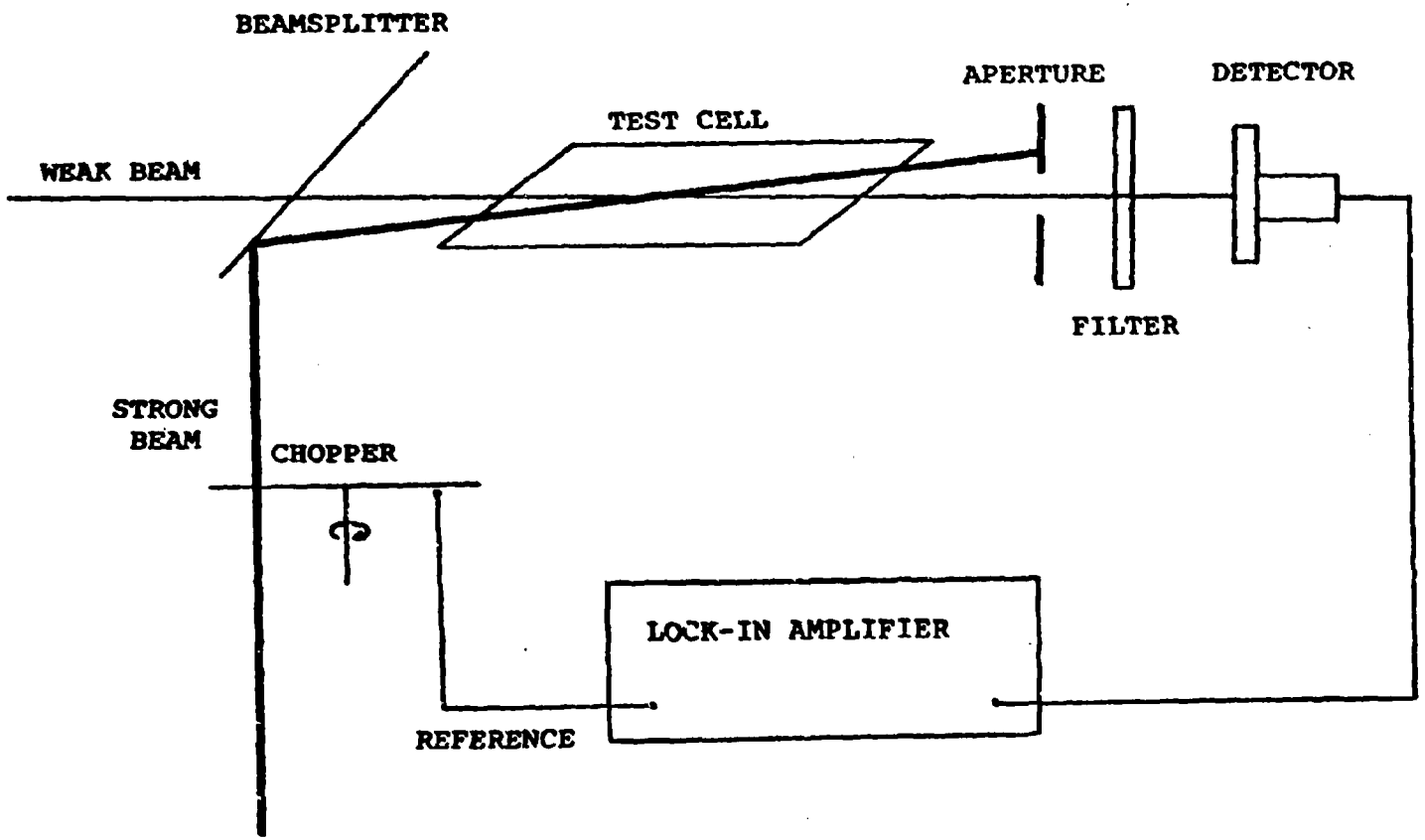

FIGURE 5.1 - EXPERIMENTAL SCHEME FOR LIFETIME DETERMINATIONS

the population densities of the two states. The delayed weak pulse, from the variable length arm of the interferometer, is amplified by the medium according to (5.6). By monitoring the weak beam intensity as a function of time delay it is possible to extract the quantities A_1, A_2, B_1, and B_2 using a least squares fit analysis.

In the experiment, the relative intensities of the two beams are determined by the reflectance coefficients of the two beamsplitters in the interferometer. Ratios of 300:1 or 20:1 were used. One of the great advantages of this time measurement technique is its ability to use a relatively slow, inexpensive detector for the intensity measurement. A UDT.500 photodiode was used. This generated signal strengths of ≈20 μV to 1 mV from the weak beam. An interference filter was used to transmit only those wavelengths in a 20 Å band around the laser wavelength.

The angle between the beams is greatly exaggerated in the diagram. It was made as small as possible in order to maximize the interaction volume. The test cell was placed near the beamsplitter shown in the figure to allow a long path length for the two optical beams to separate. An aperture blocked the strong beam while transmitting the weak one.

A 30 Hz synchronous motor driving a single-bladed chopper wheel modulated the strong beam. The signal was fed into a P.A.R. HR-8 Lock-In Amplifier in order to remove those components of the signal not due to the transient

optical perturbation. A reference for the lock-in was provided by a small lamp and photodiode, also modulated by the chopper. The output of the lock-in was fed to a chart recorder and the digital data acquisition system for later computer analysis.

The evolution of the population densities due to the transit of the strong pulse is shown in the upper curves of Figure 5.2. If the FWHM of the laser pulse is T and the strong pulse peak occurs at t_0 then the perturbation can be expected to last from t_0-T to t_0+T. Afterwards, the only contribution to the population difference will be the relaxation mechanisms of the upper and lower states. The small signal gain will be proportional to this population difference at time delay τ, $n_2(\tau)-n_1(\tau)$. The lower curve in the figure is the expected behavior of the intensity of the weak beam as a function of time delay. The weak beam will be amplified to I_0 by the initial population difference. The subsequent perturbation will decrease the gain, so that the intensity is reduced to $I_0-\Delta I_0$. The signal will then regain intensity according to (5.6).

5.2 The Argon Ion Laser Lower State Lifetime Experiment

The lifetimes of the lower states of laser transitions are particularly important in maintaining the population inversion necessary for light amplification[36]. While the

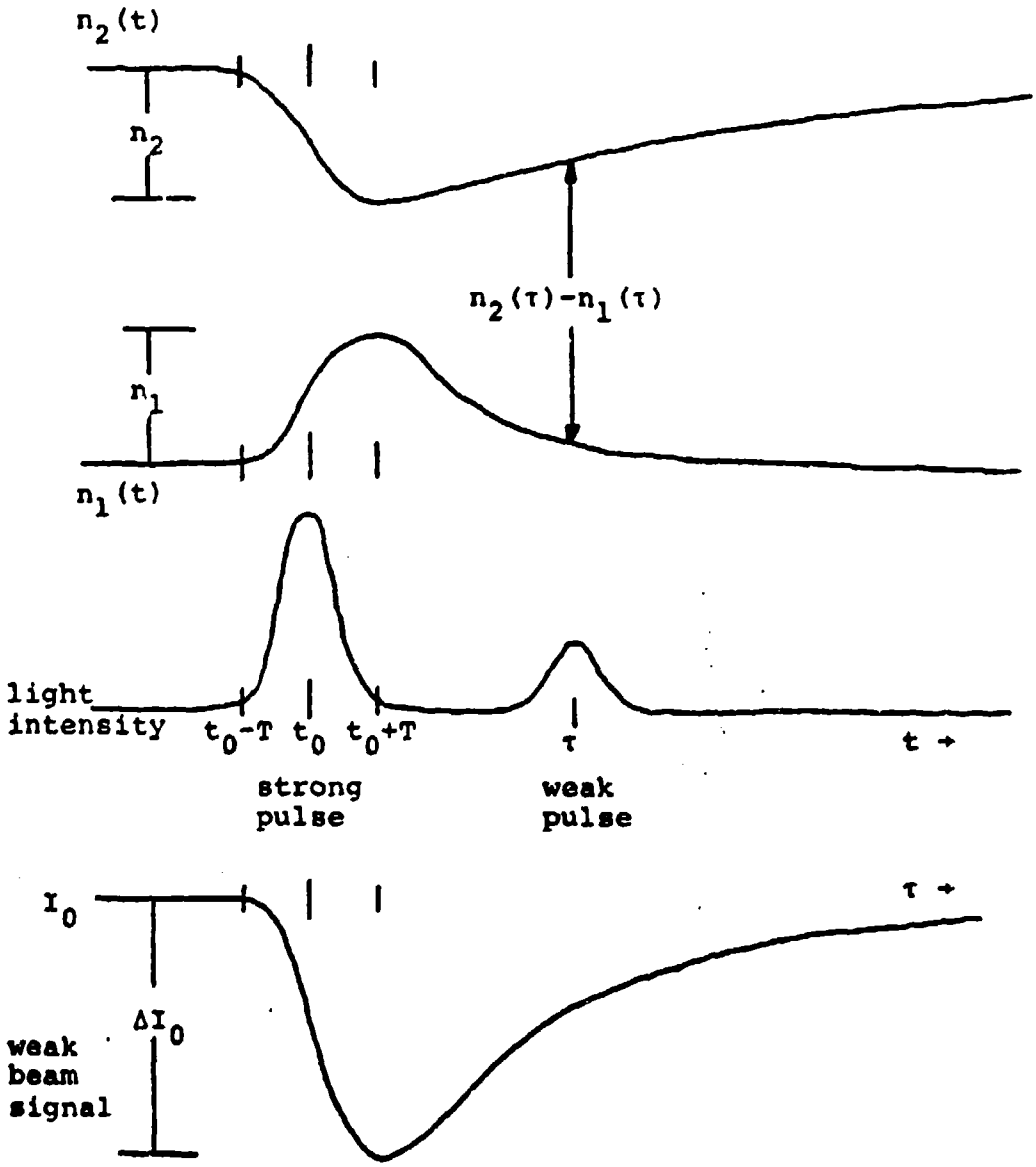

FIGURE 5.2 - EVOLUTION OF POPULATION DENSITIES DUE TO STRONG PULSE PERTURBATION (upper curves) AND WEAK BEAM INTENSITY AS A FUNCTION OF TIME DELAY (lower curve)

lifetimes of the upper states of the argon ion laser lines have been measured using optical[37] and electron impact[38] perturbations, the relaxations of the lower levels occur more rapidly and have defied direct measurement.

The choice of laser transition used in this experiment bears careful consideration. The 4s $^2P_{1/2}$ and 4s $^2P_{3/2}$ are predicted to have similar lifetimes[9] and are both strong candidates for study. The $^2P_{3/2}$ state terminates the extremely powerful 4880 Å and 5145 Å lines while the $^2P_{1/2}$ state is the lower level of the 4765 Å and 4965 Å lines, which are nearly as strong.

Gain at 4880 Å is four to six times that of the other lines under conditions typical of an argon ion laser discharge (current densities of 200-450 A/cm^2 and pressures of 0.4-1.2 torr)[39]. Thus, the signal strength in the gain experiment will be correspondingly greater at this wavelength for an equal perturbation of the populations. For an amplification length of 40 cm, the gain at 4880 Å is 20% to 60%, depending on the discharge conditions. Of course, large gain makes mode locking difficult. In fact, the argon ion laser is not generally capable of mode locked operation using commercially available components.

The mode locker circuitry was modified, however, to facilitate cavity dumped operation, as explained in Chapter 4. The ENI 300L amplifier produces higher radio frequency power levels than does the Spectra Physics Model 365 driver originally supplied. Using ≥3 W of applied rf power, the

laser system could be mode locked at 4880 Å under conditions of moderate gain (≈30% per pass using laser currents of ≈20 A).

The larger gain at 4880 Å causes pulse durations comparable to those measured at 5145 Å at higher currents. The output power is reduced, however, to ≈25% of that attained at 5145 Å. The weak beam intensity must be maintained at a level below the saturation intensity of the transition for the small signal gain analysis to apply. Large power densities in the strong beam are desired in order to effect large perturbations in the population densities. A measure of the amount by which the populations will be perturbed is the saturation intensity[25],

$$I_s = \frac{2\pi hcA_1A_2}{\lambda^3 A_{21}} . \qquad (5.7)$$

The rates A_2 and A_{21} have been experimentally determined. Bennett et al[38] measured the lifetime of the 4p $^2D^{\circ}_{5/2}$ upper state of the 4880 Å line to be 9.1±0.6 nsec. The ratio A_2/A_{21} was determined to be 1.29 at this wavelength[40]. The lower state lifetime has been calculated to be 0.36 nsec[9] and can be inferred from experimental determinations of the Lorentz width of transitions to that state[27,41-43]. Sze and Bennett[27] determined that the natural width at 4880 Å is 486 MHz. The natural width, $\Delta\nu_n=(A_1+A_2)/2\pi$, can be used to obtain the lower state lifetime. Using the above values, $A_1=2.94\times10^9$. Thus, the $^2P_{3/2}$ state has a lifetime of ≈1/3 nsec.

These numbers can be used to determine the saturation intensity. The calculated values for each of the four laser wavelengths is summarized in Table 5.1. Included, also, are the approximate values of small signal gain in the investigation discharge[39], rf powers required for mode locking, and peak powers of the pulses.

Wavelength (Å)	4880	5145	4765	4965
Lower State	$^2P_{3/2}$	$^2P_{3/2}$	$^2P_{1/2}$	$^2P_{1/2}$
Saturation Intensity (W/cm^2)	4.2	50	6.4	8.9
Small Signal Gain at 20 A (%/pass)	30	5	7	5
Mode Locking Power (W)	4	0.3	0.3	0.3
Peak Power of Mode Locked Pulses (W)	25	100	30	30

TABLE 5.1 - PERTINENT CHARACTERISTICS OF THE STRONG ARGON ION LASER TRANSITIONS

The saturation intensities must be greatly exceeded for significant perturbation to occur. It is apparent, however, that an order of magnitude more power is needed at 5145 Å than at the other wavelengths. Thus, 4880 Å is the preferred transition for the lifetime experiment.

Beamsplitters of 6% transmittance at 45° incidence for "s" polarized, ≈5000 Å light were installed in the interferometer to provide a strong beam peak intensity of

≈1 KW/cm^2 and power densities of ≈3 W/cm^2 in the weak beam. The spot size at the investigation tube was 2 mm.

The discharge tube was a Laser Sciences Model 252 argon ion laser, with the cavity optics removed. This is a transportable system, with a self-contained heat exchanger and a photo-feedback regulated power supply. In normal operation as a CW laser it was capable of 2½ W output when oscillating on all lines.

Because this is a sealed off tube, the argon pressure could not be varied, and, in fact, was not precisely known. Because the unit was capable of high output powers, however, the pressure was probably in the 0.5 to 1.0 torr range. Also, because of the relatively large gain available, large gain perturbations were anticipated. Unfortunately, the power supply only provided photo-feedback regulation. Thus, when the unit was not used as a laser, the supply would increase the discharge current to the maximum level. A circuit was installed to vary this level between 14 and 20 A. The current was unregulated, however, and created noisy discharge conditions.

The process of aligning the laser beams was exceedingly difficult. First, the interferometer track was adjusted to minimize sagging. Even with painstaking care, the residual deviations of the support shafts caused the weak beam to wander ±0.5 mm vertically over the 2 m path length necessary to separate the crossed beams at the detector.

This separation could be made as large as 5 mm. Because the weak beam size was ≈2½ mm, a 4 mm aperture was placed in front of the detector to isolate the weak beam. Only 3% of the detector signal was due to scattered light from the strong beam, even though it was 300 times as powerful as the weak beam. The scattering was due to the strong beam passing through the narrow tube bore.

Unfortunately, there was insufficient signal strength for a lifetime determination, despite the great intensity of the mode locked, cavity dumped pulses and the large gain at 4880 Å available in the discharge tube. In fact, no signal could be detected which could be attributed to the expected gain perturbation.

The lack of signal is probably due to insufficient perturbation of the population densities by the strong pulse. While the single pass gain of the amplifier approached 30%, the change in this value could be much smaller, depending on the fraction of the population which is perturbed. Also, the crossed beams undoubtably reduced the interaction volume within the discharge by a factor of one-half or more. Thus, the signal may have been represented by changes in weak beam intensity on the order of 1%.

The noise in the system was primarily caused by vibrations of the mirrors on the variable length arm of the interferometer. The average power of the mode locked laser

pulses was monitored and did not fluctuate over the one second averaging time used in the experiment. The lock-in amplifier should have removed any noise due to fluctuations in the gain of the discharge. However, a 30 Hz component of noise can exist from the combination of the weak beam and scattered light from the chopped strong beam on the detector.

The detector will sum and square the electric fields of the two waves. If the weak beam contains noise, so will the signal. As the weak beam passes through the long, narrow discharge tube, it may be partially blocked if not precisely aligned. This will occur if the mirrors on the translation stage vibrate with an amplitude of $\sim 10^{-4}$ radians. The signal contains a 30 Hz component of noise which may exceed the $\sim$1% intensity variations expected from the gain measurement.

Future experiments could profit from a more stable time delay track. The present apparatus could be modified by installing shorter, more rigid, support shafts. In addition, a larger bore investigation tube would be preferable, as would a current regulated power supply.

5.3 The Sodium Salicylate Lifetime Measurement

In order to demonstrate the utility and generality of this method of determining lifetimes in the 100 μsec to 2 nsec range, the technique was applied to the measurement

of the decay time of absorbed light in the ultraviolet scintillator sodium salicylate ($C_7H_5O_3Na$). Of course, the experiment should work in absorption as well as in gain. In the case of a transition from the ground state of a molecule, as is the case, the lower state cannot decay further and has no associated time constant. This simplifies the analysis. Referring to Figure 5.2, the upper and lower state populations will be equally perturbed by the strong beam; the population is pumped from the lower state to the upper state. The relaxations of these populations should occur at the same rate. The perturbation effects an increase in transmission of the weak beam, which is detected as before in the gain experiment.

A saturated solution of sodium salicylate in ethanol was placed in a 1 cm long test cell with flat, parallel windows. The cell was tilted to approximately Brewster's angle to increase the absorption length and reduce losses due to reflections from the windows. Because of the short interaction length, the strong and weak beams could be widely separated at the detector. A spacing of 1 cm was readily attained using a path length of ≈50 cm.

Sodium salicylate in ethanol is an interesting candidate for study as it has been considered for use as amplifying medium in a tunable UV laser[44]. Unfortunately, its absorption is small at the argon laser wavelengths[45]. Observations showed that the absorption did not vary significantly with laser wavelength and was <1% for the

absorption length available. Therefore, the laser was operated at 5145 Å, the most powerful mode locked line, in order to effect the largest perturbation possible.

The interpretation of the weak beam signal requires some consideration. We must determine specifically the effects of the perturbation, relaxations, and finite width of the probe pulse. For this analysis, T represents the 1/e half-width of the Gaussian mode locked pulses, τ is the time interval between the pulses, R is the relaxation rate of the upper state, and t_0 in Figure 5.2 is set equal to zero.

At some time, t_1, the perturbation of either population density is

$$n(t_1) = n \int_{-\infty}^{t_1} e^{-(t/T)^2} e^{-R(t-t_1)} dt. \qquad (5.8)$$

The decay will start as soon as the population perturbation begins. The absorption will be proportional to this perturbation. Since the unperturbed absorption is less than 1%, however, the exponential form derived in (5.6) can be approximated, so that the absorption at t_1 can be expressed as

$$a(t_1) = a_0 \int_{-\infty}^{t_1} e^{-(t/T)^2} e^{-R(t-t_1)} dt, \qquad (5.9)$$

where a_0 is a proportionality constant. To obtain the change in intensity of the weak beam as a function of time delay, this expression must be integrated over the shape of the probing pulse. The Gaussian profile of the weak pulse is displaced by τ. Therefore, the signal will be

$$S(\tau) = S_0 \int_{-\infty}^{\infty} e^{-((t_1-\tau)/T)^2} \cdot \int_{-\infty}^{t_1} e^{-(t/T)^2} e^{-R(t-t_1)} \, dt \, dt_1, \quad (5.10)$$

where S_0 is another constant.

This function, which describes the response of the system at all time delays, cannot be evaluated analytically. During the passage of the strong pulse, when t_1 is comparable in magnitude to T, the decay term may be neglected if the lifetime is long compared with the pulse duration. The function is still transcendental, however, as it involves the integral of the error function. In Figure 5.3, the data obtained during the passage of the strong pulse has been fit to a Gaussian form using a least squares fit analysis. As can be seen from the figure, this fit is a good approximation, and corresponds to a Gaussian having a half-width at half-maximum of 268 psec.

For $t_1 >> T$, the inner part of (5.10) can be integrated using the method of completion of the square. This simplifies the expression to

$$S(\tau) = S_1 \int_{-\infty}^{\infty} e^{-((t_1-\tau)/T)^2} e^{-Rt_1} \, dt_1 \quad (5.11)$$

where S_1 is another constant of proportionality. This expression can also be evaluated analytically by completion of the square. Thus, the expression for the experimental signal at large time delays can be written as

$$S(\tau) = S_2 \, e^{-R\tau}. \quad (5.12)$$

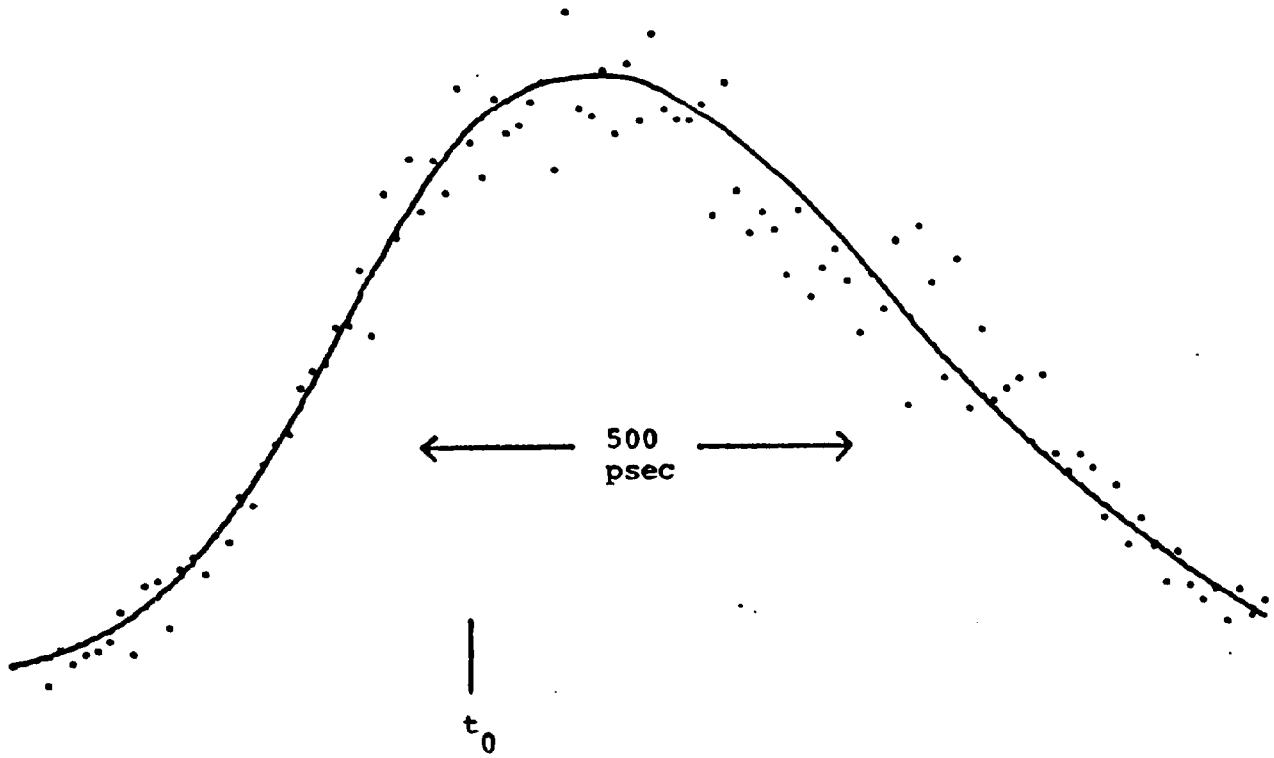

FIGURE 5.3 - SODIUM SALICYLATE LIFETIME DATA;

TRANSMISSION OF WEAK BEAM AS A FUNCTION OF TIME DELAY

The only effect the finite duration of the pulse has on the analysis of the data, then, is the length of time which must be allowed to pass before the signal corresponds to the exponential decay process.

Figure 5.3 represents ≈15 successive scans of the translation stage of the interferometer. Approximately 80 data points per scan were taken. The signals generated by individual scans were quite noisy due to the weak perturbation of the absorbing medium. Figure 5.3 was generated by averaging the ≈1200 digital data points over 15 psec intervals using a computer program.

The mode locked, cavity dumped laser was operated at a discharge current of 21 A for these measurements. Referring to Figure 4.9, the FWHM of the pulses is expected to be ≈180 psec. A least squares fit to a decaying exponential was performed, commencing at t_0 + 450 psec. The analysis yielded a decay time of 634±95 psec. Because of the complex nature of the function near the strong pulse maximum, the fit was approximated by hand in this region of the figure.

Berlman[45] has computed the natural fluorescent lifetime from the $^1S_1$ state of sodium salicylate in ethanol to be 25.6 nsec. It should be emphasized, however, that this UV scintillator is not a simple two level system. In the present experiment, we observe a decay from whichever state has been populated by the absorption of 5145 Å light, not the fluorescence from the $^1S_1$ state. Therefore, it is not

surprising that the measured decay time differs from the fluorescent lifetime. Different relaxation mechanisms are operating.

The sodium salicylate solution tended to bleach due to the intense optical radiation on time scales of five to thirty minutes. This limited both the intensity of the strong pulse and the number of absorption measurements. Several runs, however, reproduced the characteristics of Figure 5.3, demonstrating the reliability of the technique.

The measurement of the relaxation time of a fast decay process in sodium salicylate demonstrates the utility of the method of lifetime determinations by time-dependent gain or absorption measurements.

APPENDIX I - Acousto-Optical Interactions

Diffractive light modulation by means of elastic waves[46] has proven to be useful in mode locking[6,47] and cavity dumping[30] operations. Theoretical descriptions of the acousto-optical interaction using several different approaches have been previously presented[12-15,28,29,48]. In this appendix, however, Bragg diffraction is analyzed using classical wave theory.

For these discussions, λ, ω, and k represent the optical wavelength, frequency, and wavevector; Λ, Ω, and K are these same quantities for the acoustic wave. For the preliminary analyses, the optical beam is assumed to have a rectangular profile of width 2w.

I.1 Acousto-Optical Mode Locking

Figure I.1 illustrates mode locking of a CW laser by active loss modulation. In this case, the optical and acoustic waves are normal to each other. Uniform loss across the width, 2w, of the light beam is ensured by the use of an acoustic standing wave which has a very small wavelength compared to the cross-sectional dimension of the optical beam.

Light entering an elasto-optical grating described by an index of refraction

$$\eta(x,t) = \eta_0 + 2\eta_1\cos(\Omega t)\sin(Kx) \qquad (I.1)$$

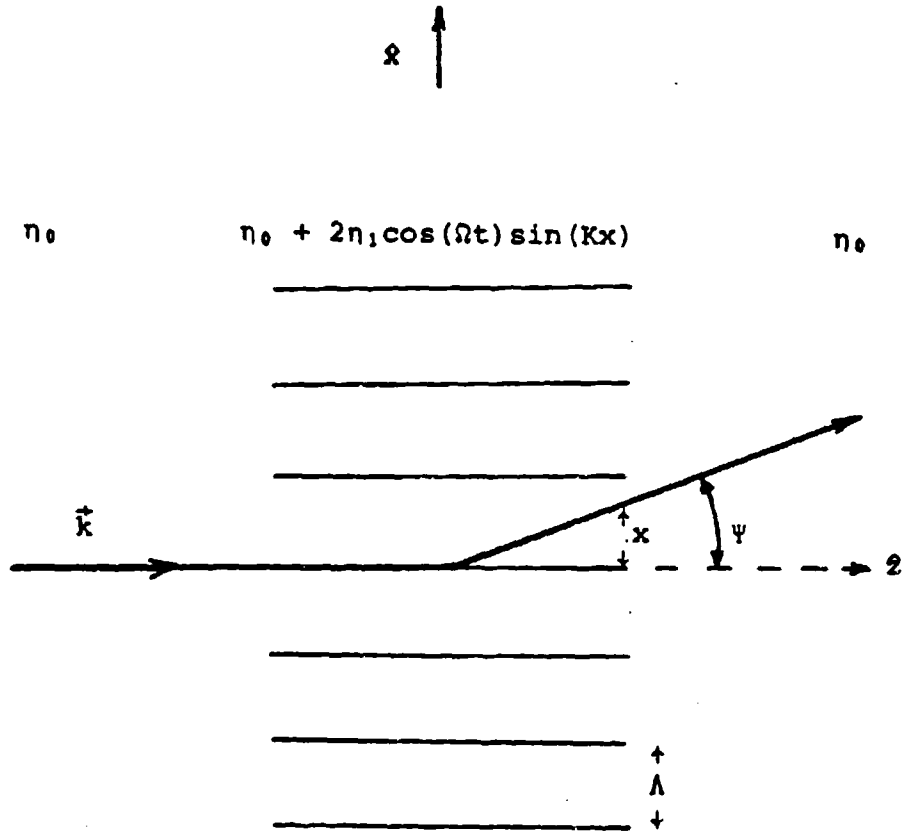

FIGURE I.1 - DIFFRACTIVE LOSS MODULATION BY A STANDING ACOUSTIC WAVE

experiences a phase shift

$$\Delta\phi = k\eta_0 x \sin\Psi + 2k\eta_1 L \cos(\Omega t)\sin(Kx) \qquad (I.2)$$

where L is the interaction length and Ψ is the direction of the emergent light. The angular distribution of the diffracted light is expressible as

$$E(\Psi) = C\, e^{i\omega t} \int_{-w}^{w} e^{i\Delta\phi}\, dx \qquad (I.3)$$

where C is a constant to be determined later.

Making use of the identity[49]

$$\exp\{iA \sin B\} = \sum_{p=-\infty}^{\infty} J_p(A)\, e^{ipB} \qquad (I.4)$$

the angular distribution can be rewritten as

$$E(\Psi) = 2C\, e^{i\omega t} \sum_{p=-\infty}^{\infty} J_p[2k\eta_1 L\cos(\Omega t)] \cdot \left\{\frac{\sin[(pK+k\sin\Psi)w]}{pK+k\sin\Psi}\right\} \qquad (I.5)$$

after integration. Normalization is based on the requirement that $|E(\Psi=0)|=E_0$ when $\eta_1=0$. Also, we use the fact that

$$\begin{aligned} J_0(0) &= 1 \\ J_p(0) &= 0 \text{ for all } p \neq 0 \end{aligned} \qquad (I.6)$$

and

$$\frac{\sin(pKw)}{pK} \xrightarrow[p\to 0]{} w. \qquad (I.7)$$

Consequently, only the p=0 term in the series is non-vanishing and the normalization requirement is

$$C = \frac{E_0}{2w} . \tag{I.8}$$

Thus, the field can be written as

$$E(\Psi) = E_0 e^{i\omega t} \sum_{p=-\infty}^{\infty} J_p[2kn_1 L\cos(\Omega t)] \cdot \left\{\frac{\sin[(pK+k\sin\Psi)w]}{pK+k\sin\Psi}\right\} . \tag{I.9}$$

For $w \neq 0$, the argument of the sine term in the above equation is always finite when

$$\Psi = \sin^{-1}\left(\frac{p\lambda}{\Lambda}\right). \tag{I.10}$$

Therefore, the field diffracted into each order, p, is

$$E_p = E_0 \; J_p[2kn_1 L \cos(\Omega t)] \; e^{i\omega t} \tag{I.11}$$

and the intensity is

$$I_p = E_0^2 \; J_p^2[2kn_1 L \cos(\Omega t)]. \tag{I.12}$$

The optical loss is a periodic function of time for the $p=0$ order. If the acoustic frequency, Ω, can be synchronized to the laser cavity resonance, this mechanism can be effective for loss modulated mode locking.

In reality, the optical beam will not have a rectangular profile. For the TEM_{00} mode the beam intensity has a Gaussian form,

$$I(x) = E_0^2 \; e^{-\left(\frac{x}{a}\right)^2} \tag{I.13}$$

where a = 0.4 mm in a typical mode locked argon ion laser.

The bore of the discharge tube effectively limits the extent of the beam to a half-width of w = 0.8 mm, beyond which the field may be considered to be zero.

The Gaussian beam profile may be incorporated into (I.3) to obtain

$$E(\Psi) = C' \, e^{i\omega t} \int_{-w}^{w} e^{i\Delta\phi} \, e^{-\left(\frac{x}{a}\right)^2} dx. \qquad \text{(I.14)}$$

This can be expanded to

$$E(\Psi) = C' \, e^{i\omega t} \left\{ \int_{-w}^{w} \cos(\Delta\phi) \, \exp\left(-\frac{x^2}{2a^2}\right) dx \right.$$
$$\left. + \, i \int_{-w}^{w} \sin(\Delta\phi) \, \exp\left(-\frac{x^2}{2a^2}\right) dx \right\} \qquad \text{(I.15)}$$

which yields

$$I(\Psi) = C_0 \left\{ \left\{ \int_{-w}^{w} \cos(\Delta\phi) \, \exp\left(-\frac{x^2}{2a^2}\right) dx \right\}^2 \right.$$
$$\left. + \left\{ \int_{-w}^{w} \sin(\Delta\phi) \, \exp\left(-\frac{x^2}{2a^2}\right) dx \right\}^2 \right\} \qquad \text{(I.16)}$$

for the intensity distribution. This expression has been numerically integrated using a computer program containing parameters pertinent to the mode locker used in these studies.

The diffraction pattern is plotted for angles of up to ±3.5 milliradians in Figure I.2. The upper figure is for the case of minimum diffraction, that is $\Omega t = \pi/2$. The lower plot shows the case for $\Omega t = 0$, or maximum diffraction. The ordinate in both cases is calibrated in the same intensity units.

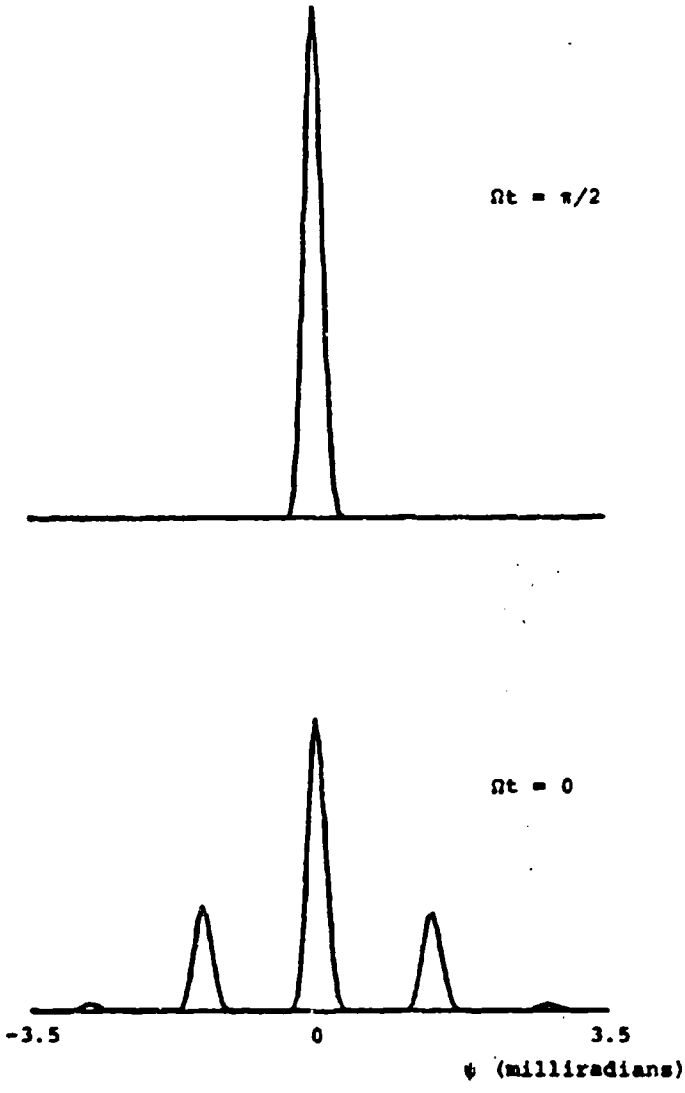

FIGURE I.2 - MODE LOCKER DIFFRACTION PATTERN

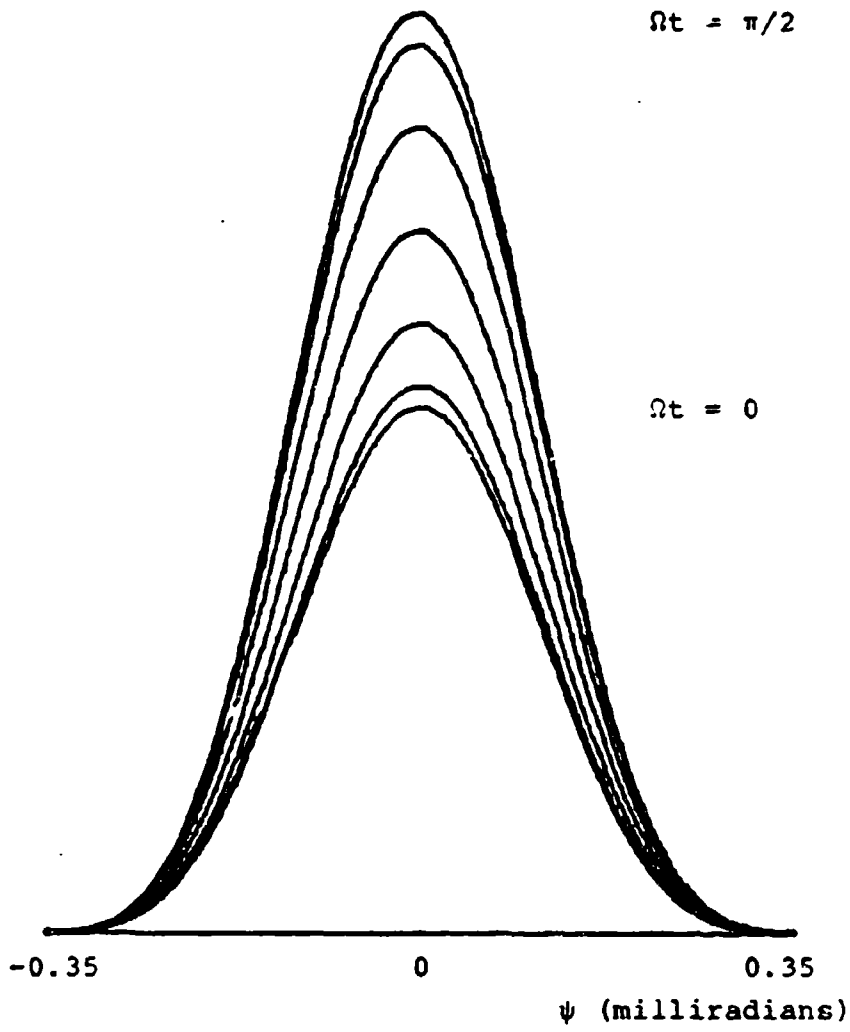

FIGURE I.3 - MODE LOCKED DIFFRACTION PATTERN
CENTRAL PEAK AS A FUNCTION OF TIME

Figure I.3 is a plot of the central diffraction peak from -0.35 to 0.35 milliradians as a function of time. The seven curves show the transmitted intensity for $\Omega t=0$ to $\pi/2$ in increments of $\pi/12$ (bottom to top). At maximum loss, the transmitted beam has only 57% of the intensity of an undiffracted beam. This agrees with the analysis of the rectangular beam profile, which predicts 58% transmission.

I.2 Acousto-Optical Cavity Dumping

In the case of cavity dumping, light polarized with the electric field in the y-direction propagates as shown in Figure I.4. A traveling acoustic wave causes the index of refraction to vary as

$$\eta(x,t) = \eta_0 + \eta_1 \sin(Kx-\Omega t). \tag{I.17}$$

The electric field may be written as

$$E = F(x,z,t)\ e^{i\omega t}\ e^{i\eta_0 \vec{k}\cdot\vec{r}} \tag{I.18}$$

where $F(x,z,t)$ varies slowly compared to $e^{i\omega t}$ and $e^{i\eta_0\vec{k}\cdot\vec{r}}$. The periodicity in the index of refraction manifests itself as a periodic structure in $F(x,z,t)$. In fact, $F(x,z,t)$ can be written as a Fourier series

$$F(x,z,t) = \sum_{p=-\infty}^{\infty} f_p(z)\ e^{ip(Kx-\Omega t)}. \tag{I.19}$$

Thus,

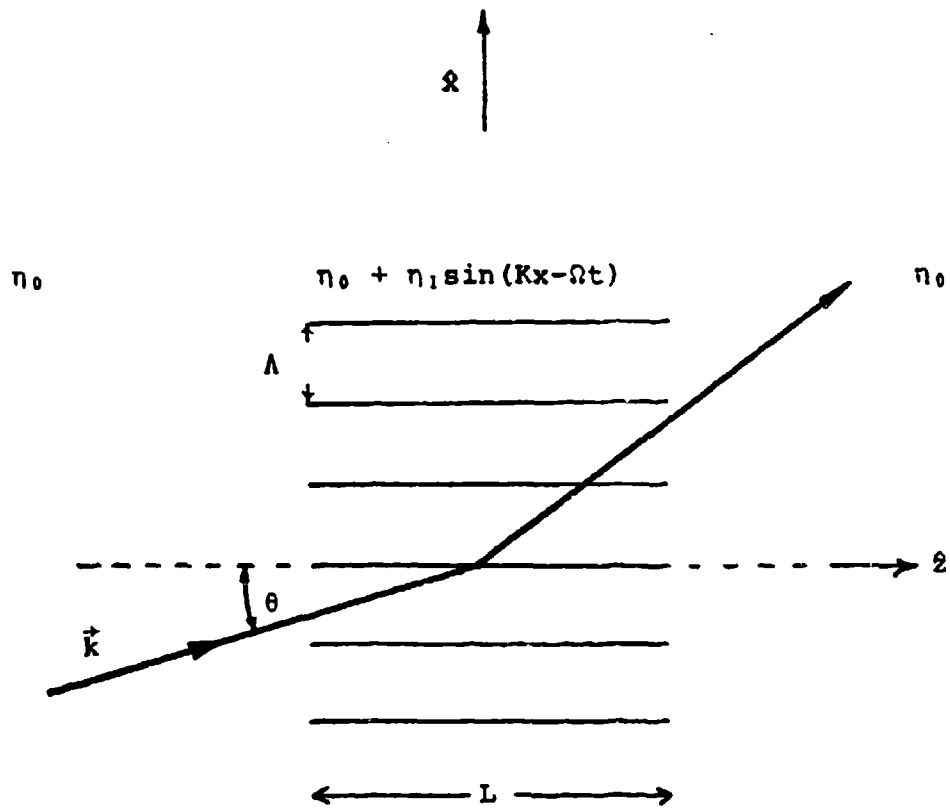

FIGURE I.4 - ACOUSTO-OPTICAL DEFLECTION BY A TRAVELING WAVE

$$E = e^{i\omega t}\, e^{in_0\vec{k}\cdot\vec{r}} \sum_{p=-\infty}^{\infty} f_p(z)\, e^{ip(Kx-\Omega t)}. \qquad (I.20)$$

For the case illustrated in Figure I.4

$$\vec{k}\cdot\vec{r} = kz\cos\theta + kx\sin\theta. \qquad (I.21)$$

The expression for the electric field can be inserted into the wave equation

$$\nabla^2 E = \left\{\frac{n(x,t)}{c}\right\}^2 \frac{\partial^2 E}{\partial t^2} \qquad (I.22)$$

which, in this case, reduces to

$$\frac{\partial^2 E}{\partial x^2} + \frac{\partial^2 E}{\partial z^2} = \left\{\frac{n(x,t)}{c}\right\}^2 \frac{\partial^2 E}{\partial t^2}. \qquad (I.23)$$

Differentiation yields

$$\frac{\partial^2 E}{\partial x^2} = -e^{i\omega t} \sum_{-\infty}^{\infty} [kn_0\sin\theta + pK]^2 f_p \cdot e^{in_0\vec{k}\cdot\vec{r}}\, e^{ip(Kx-\Omega t)} \qquad (I.24)$$

$$\frac{\partial^2 E}{\partial z^2} = e^{i\omega t} \sum_{-\infty}^{\infty} [f_p'' + 2ikn_0 f_p'\cos\theta - k^2 n_0^2 f_p \cos^2\theta] \cdot e^{in_0\vec{k}\cdot\vec{r}}\, e^{ip(Kx-\Omega t)} \qquad (I.25)$$

$$\frac{\partial^2 E}{\partial t^2} = -e^{i\omega t} \sum_{-\infty}^{\infty} [\omega + p\Omega]^2 f_p\, e^{in_0\vec{k}\cdot\vec{r}} \qquad (I.26)$$

where $f_p' = \frac{\partial f}{\partial z}p$. Neglecting terms of order $\frac{\Omega}{\omega} \sim 10^{-6}$ and $n_1^2 \sim 10^{-10}$, introduction of the above derivatives into the wave equation gives

$$\sum_{-\infty}^{\infty}\{f_p''-2in_0kf_p'-k^2n_0^2f_p-2pn_0kKf_p\sin\theta-p^2K^2f_p\}$$

$$\cdot e^{in_0\vec{k}\cdot\vec{r}}\, e^{i\omega t}$$

$$=\sum_{-\infty}^{\infty}\{n_0^2k^2f_p-in_0n_1k^2[e^{i(Kx-\Omega t)}-e^{-i(Kx-\Omega t)}]\}$$

$$\cdot e^{in_0\vec{k}\cdot\vec{r}}\, e^{i\omega t}. \qquad (I.27)$$

Noting that for $\theta<<1$ ($\cos\theta\approx1$) a recurrence relationship is obtained, where

$$f_p''-2ikn_0f_p'-[2pn_0kK\sin\theta+p^2K^2]f_p$$

$$= in_0n_1k^2[f_{p-1}-f_{p+1}] \qquad (I.28)$$

Since $k \sim 10^5$, the first term is negligible;

$$f_p'+\frac{n_1k}{2}[f_{p-1}-f_{p+1}]= i\frac{[p^2K^2+2pn_0kK\sin\theta]}{2kn_0}f_p. \qquad (I.29)$$

It is convenient to define the following parameters:

$$v = n_1kL$$

$$Q = \frac{K^2L}{n_0k} \qquad (I.30)$$

$$\alpha = -\frac{n_0k}{K}\sin\theta$$

to obtain

$$f_p' + \frac{v}{2L}[f_{p-1}-f_{p+1}] = \frac{ipQ}{2L}(p-2\alpha)\, f_p. \qquad (I.31)$$

The appropriate boundary condition is that at $z=0$ the light is not yet deflected and is, therefore, in the $p=0$ order;

$$f_0(0) = E_0$$

$$f_p(0) = 0 \text{ for all } p \neq 0. \qquad (I.32)$$

For light to be diffracted into order p, it must be in phase with the p=0 order light. Thus, the coefficient of the right-hand side of (I.31) must be zero. This condition is satisfied when

$$\sin\theta = -\frac{pK}{2\eta_0 k} . \qquad (I.33)$$

Also, only those orders differing by p=±1 may be directly coupled. If the angle of incidence is constrained such that $\alpha=\frac{1}{2}$ (the Bragg angle), then we are concerned only with light in the p=0 and p=1 orders. Using these conditions, the recurrence relationship becomes

$$f_0' - \frac{v}{2L} f_1 = 0$$

$$f_1' + \frac{v}{2L} f_0 = 0. \qquad (I.34)$$

The solutions to these equations are

$$f_0 = -E_0 \cos\left(\frac{vz}{2L}\right)$$

$$f_1 = E_0 \sin\left(\frac{vz}{2L}\right). \qquad (I.35)$$

Thus, the intensities at z=L are

$$I_0 = E_0^2 \cos^2(v/2)$$

$$I_1 = E_0^2 \sin^2(v/2). \qquad (I.36)$$

For $v=\pi$, all light will be deflected into the p=1 order. For the case of the cavity dumper used the acoustic power coupled into the fused quartz medium is sufficient to alter the index of refraction such that $v \lesssim 4$. Hence,

by judicious choice of operating parameters, acousto-optical deflection by means of a traveling wave can be used in cavity dumping.

APPENDIX II - The Laser Sciences Model 254 Laser

This appendix describes the design, operation, and maintenance of the Laser Sciences Model 254 argon ion laser and power supply used to generate the mode locked pulses. This prototype unit (serial number 001) was designed by the manufacturer to output 4 W CW on all lines in the blue-green part of the argon ion laser spectrum. Many modifications to the system were necessary, however, for safe and reliable operation of the laser.

II.1 Design

The plasma tube and header assembly are made of bonded BeO sections. The bore is 2½ mm in diameter, with four smaller diameter return paths bored through the plasma tube wall[50]. BeO is chosen for noble gas ion discharge tubes because of its high heat conductivity and structural strength. The tube is immersed in filtered tap water, flowing at 1½ gals/min, which dissipates the 5-10 KW of heat generated under typical operating conditions. A solenoid, developing a field of ≈1000 gauss, is also cooled.

The header contains a Philips Elmet PM-20 barium impregnated tungsten cathode; it may be reactivated after exposure to air when cold. The header also contained two barium getters. One, however, was fired by Laser Sciences

when the tube was originally sealed off. The second getter was fired after ∿500 hours of use. As no reservoir of argon was provided, the discharge tube was connected to a vacuum system to facilitate refilling.

The power supply requires 208 V, 3-ϕ input and contains a regulated discharge current supply which maintains the current level over input voltage variations of ±10%. The buck-boost transformer, T1 in the main chassis circuit diagram (Figure II.1), permits variation of the input voltage to the supply to compensate for varying line voltages and electrical loads (the effective load impedance changes with argon pressure).

Regulation is provided by 18 pairs of 2N3773 or 2N6259 (preferred) transistors in parallel (Q1,2, A-R) in the pass stage. A voltage, developed across a 1/12 Ω resistance (R1, A-F) in series with the laser is fed to A4 on the Current Control Card (PC2). A4 drives the bases of the regulating transistors through Q3-Q6. A reference voltage for A4 is derived on the Photo-Control Card (PC1). With S3 in the current feedback position (I), a constant voltage, supplied by zener diode CR1, provides a reference level for current regulation. When S3 is in the light feedback position (ϕ), the reference signal is generated by the photodiode, ES-71.

The solenoid supply is unregulated, delivering 2.75 A to the 100 Ω coil. The 1000 gauss magnetic field produced confines the electrons to the center of the bore. The

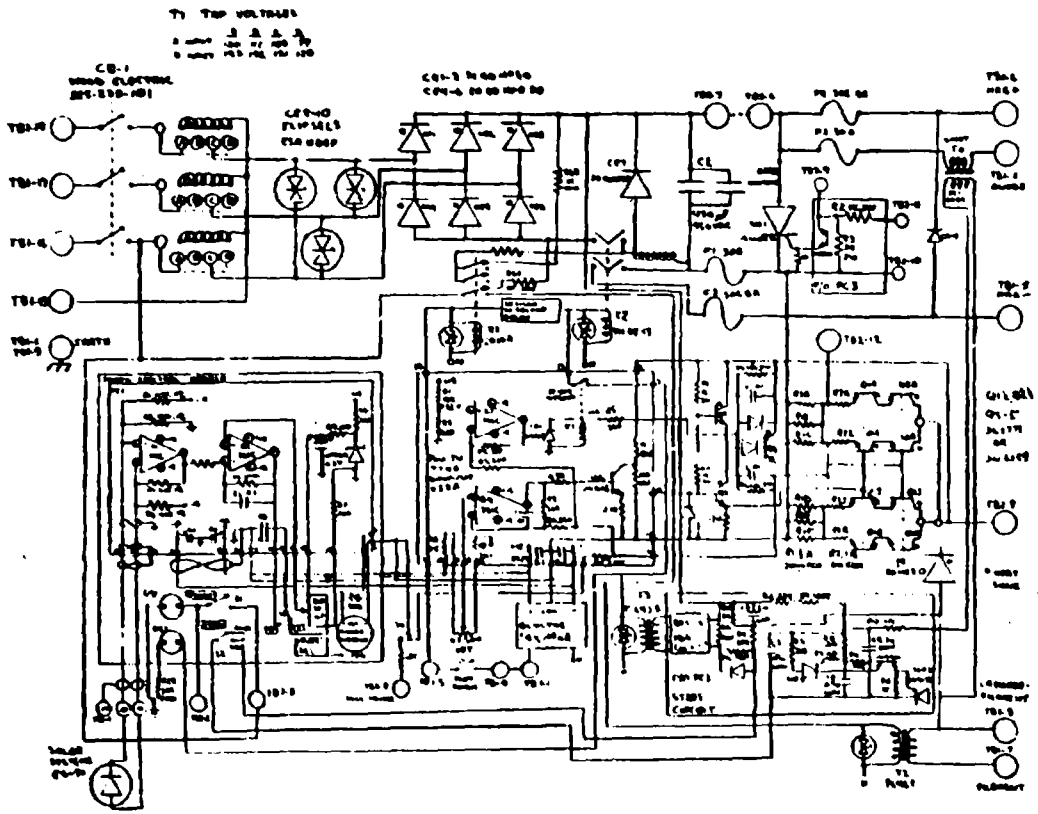

FIGURE II.1 - LASER SCIENCES MODEL 254 POWER SUPPLY

MAIN CHASSIS CIRCUIT DIAGRAM

THIS PAGE IS BEST QUALITY PRACTICABLE
FROM COPY FURNISHED TO DDC

30 A (AC) filament current is supplied by T2. This supply is turned on first. All other supplies are delayed by 30 seconds by the Artisan Time Capsule to allow the cathode to reach operating temperature before initiation of the discharge.

The Start Circuit (PC3) provides a >5000 V pulse of 1 μsec duration to the anode supply through T4. In addition, a Mid-Range Supply, also on PC3, raises the DC supply to 600 V. This maintains the discharge immediately after the start pulse is fired. With the "start" switch in the "auto" position, pulses are generated at ≈3 Hz.

The Crowbar Circuit was designed to protect the pass transistors from high voltages. When the pass voltage (TB2-8) reaches 135 V, CR-1 fires and shorts out both the pass stage and laser tube. The 30 A fuse, F1, blows. F1 and F2 were intended to provide protection for the discharge tube against large currents.

This proved to be an inadequate safeguard. A failure of the current regulation circuitry could drive dangerously high currents through the tube before the fuses had enough time to blow. Such a failure did occur, with discharge currents exceeding 50 A. The thermal shock cracked the BeO tube at a joint and destroyed tube number 002.

To prevent reoccurrences of this type, the Laser Protective Network, diagrammed in Figure II.2, was constructed. The anode current is passed through the heavy

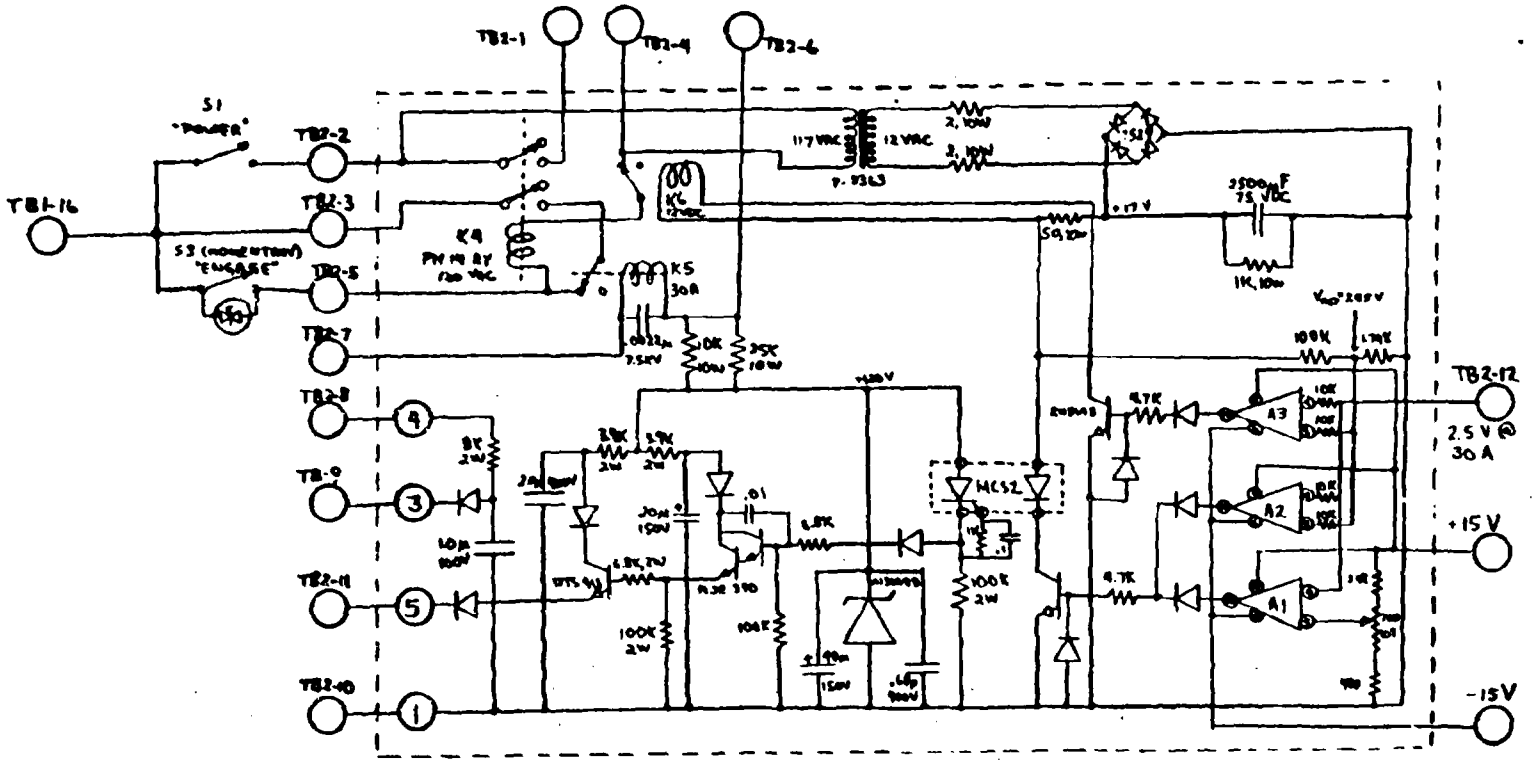

FIGURE II.2 - PROTECTIVE NETWORK CIRCUIT DIAGRAM

windings of the primary of relay K5. Currents of more than 35 A close the relay, shutting off the power supply. A faster mechanism, though not as reliable due to its many electronic components, is provided by the comparators, A1-3. These sense the current passing through R1 in the main chassis. A1 and A2 fire the Crowbar Circuit should the current exceed 30½ A or an adjustable lower amount. This mechanism actuates within microseconds. A3 also senses the current and turns off the input power should the level exceed 30½ A. In addition, the circuit breaker, CB-1, was replaced by a model having a magnetic rather than a thermal tripping mechanism.

An interlock shuts off the power when the water flow is insufficient. The flow switch, in series with the 10 micron water filter, should be set at 1.5 gals/min.

II.2 Operation

This section outlines the normal operating procedures to be followed when using the 254 laser. The controls specified, on the main chassis front panel, are shown in Figure II.3.

In order to turn the laser on:

1. It is essential that the Nupro valve connecting the discharge tube to the vacuum system and external getter bottle is closed. Otherwise, argon will expand as the cathode is heated, reducing the effective pressure

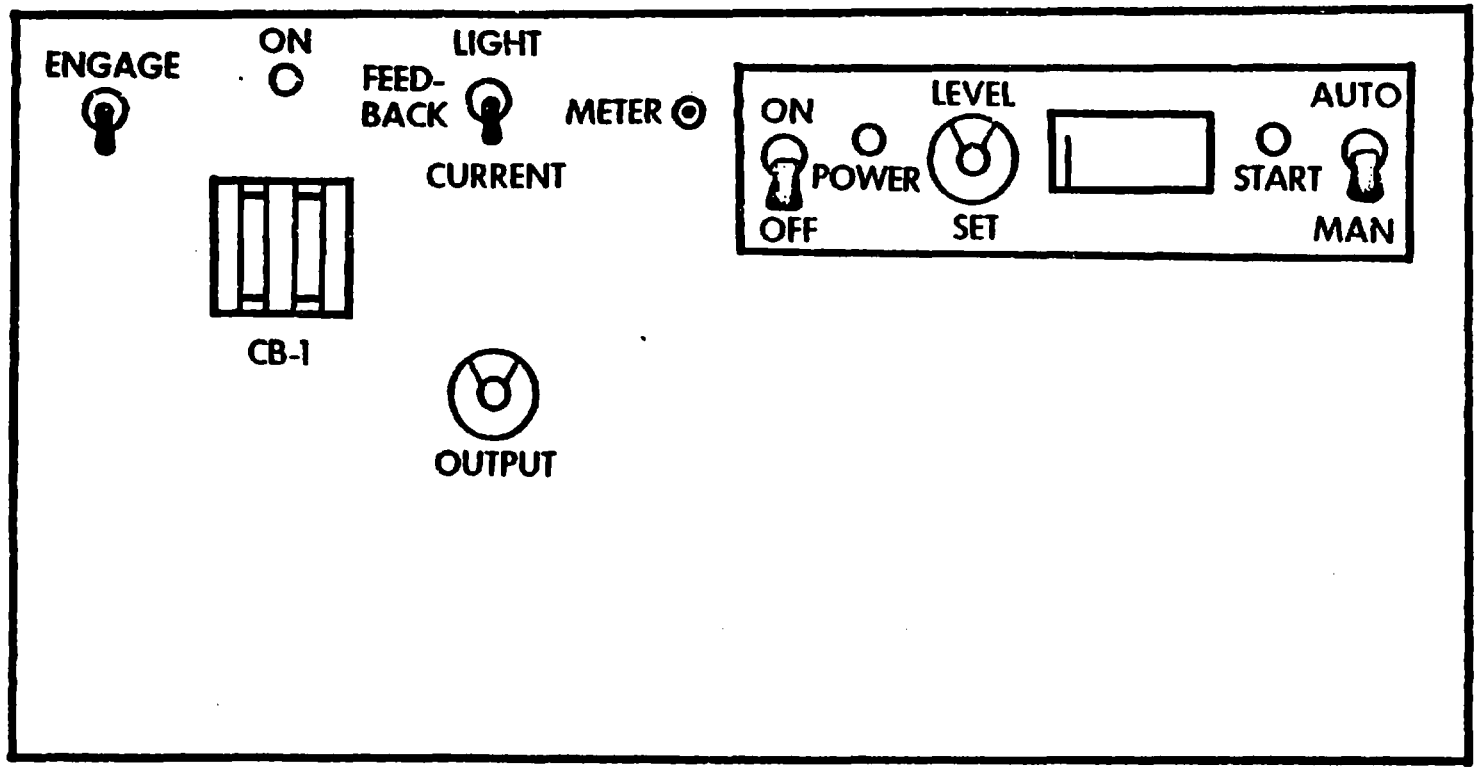

FIGURE II.3 - MAIN POWER SUPPLY FRONT PANEL

within the tube. Initiating the arc discharge becomes increasingly difficult as the pressure is lowered. In addition, when the discharge does start, the extreme heat drives the argon from the tube. The rapid variation in load impedance may cause the supply to operate outside the regulating regime.

2. Turn on the cooling water. This is passed through a 10 micron filter which frequently requires replacement when the local water supply is particularly dirty. A pressurized ballast tank reduces momentary pressure drops which would affect th water flow interlock. The pressure regulator should be adjusted for 20 pounds/in^2. This maintains the necessary 1.5 gals/min flow. Extremely high pressures may damage the BeO tube.

3. Turn on the circuit breaker, the "power" switch, and the momentary "engage" toggle switch. The protective network relays are initialized and power is sent to the main power supply. The "on" indicator should light immediately, and the "start" lamp should go on in 30 seconds.

4. The feedback switch should be in the "current" position, if the external photodiode has not been previously aligned. The current feedback mode has fewer components than does the light feedback mode and is inherently more reliable.

5. For a filling pressure of 0.9 torr, the discharge

current will be maintained at 20 A (in the current feedback mode) when the "output" potentiometer is set at ≈4.0.

6. The "start" switch may be moved from the neutral position to either the "manual" or "auto" position. In "auto", start pulses are repetitively sent down the tube at ≈2 Hz.

7. The regulating mechanism works best when the voltage across the bank of pass transistors is in the 20-60 V range. An external "pass voltage" meter has been installed in a small chassis. Alternatively, the "meter" momentary push button will transfer the pass voltage to the main chassis meter, with full scale being 135 V.

8. This meter normally measures the discharge current, calibrated for 30 A full scale. In the current feedback mode, the current may be varied using the "output" potentiometer. In the light feedback mode, the "level set" control will also affect the current level.

9. It is necessary to change the voltages derived from T1 to accommodate different filling pressures while maintaining the required voltage drop across the pass stage. The supply will not regulate at lower pass stage voltages, and high voltages will fire the Crowbar Circuit.

To turn off the laser, shut off the "power" switch and then the circuit breaker. When the output water hose feels cool, the water may be turned off.

II.3 Maintenance

The Laser Sciences Model 254 differs from other common argon ion lasers only in its gas refill procedure. Otherwise, the same routine maintenance operations, such as cleaning the internal optical surfaces and replacing water filters as necessary, are required for this unit. It should be noted that neither the anode nor the cathode of the laser is at ground potential. Thus, several exposed parts of the laser are electrically "hot", including the Nupro valve between the tube and the ballast bottle.

This bottle houses a reusable barium getter which is used to clean the argon. The gas becomes contaminated during use with anode and cathode materials and will not break down under these conditions. For at least an hour prior to use, the Nupro valve should be opened to allow the gas within the tube to diffuse into the ballast bottle and be replaced with clean gas.

Refills of clean argon are generally necessary after ~30 hours of use. With all power supplies off, the tube should be evacuated to $<10^{-7}$ torr. The system is then filled with the desired pressure of argon. Low filling pressures yield higher output powers, but require larger starting pulses than do higher filling pressures. Filling pressures of 0.7 to 1.1 torr are usually appropriate. The output power will increase substantially during the first half hour of use as some of the argon is pumped into the

tube walls.

The following is a list of problems which have frequently occurred, and their probable causes:

1. Fan does not turn on. Check the water flow.

2. "Start" lamp fails to light. Check the time delay capsule. Also, ascertain that the quick-connect start switch leads are in place.

3. Discharge does not start. Check F1 and F2 for continuity (out of the circuit). Using a dentist's mirror to block the optical path, look for the bright flash of the start pulse down the tube bore with the start switch in the "auto" position. If a start pulse is observed, yet the discharge does not start, there are several possibilities.

Defective operational amplifiers A3 and A4 (and A1 and A2 if light feedback is used) can shut down the supply before the arc discharge is formed.

The laser requires a refill of fresh gas.

The start pulses are not sufficient to break down the gas. They should be at least 5000 V with a duration of ≈1 μsec. Use a high voltage probe on an oscilloscope isolated from ground to check this.

The mid-range supply is faulty. Check this with the start switch in the neutral position. The voltage should rise to ≈300 V after the "engage" switch is thrown, and jump to ≈500 V when the start light comes on.

4. Fuse F1 is blown. The pass voltage is probably too high. Change the input leads to the supply from T1 for lower voltage.

5. The supply does not regulate. There was a common tendency for the current to oscillate at ≈40KHz with an amplitude of almost 10% of the DC value. The problem was traced to the inability of A4 to supply enough current to drive Q3-5. Q6 was installed to amplify this signal.

Figure II.4 is the load characteristics of the laser tube. This is useful when using a dummy load to troubleshoot the supply.

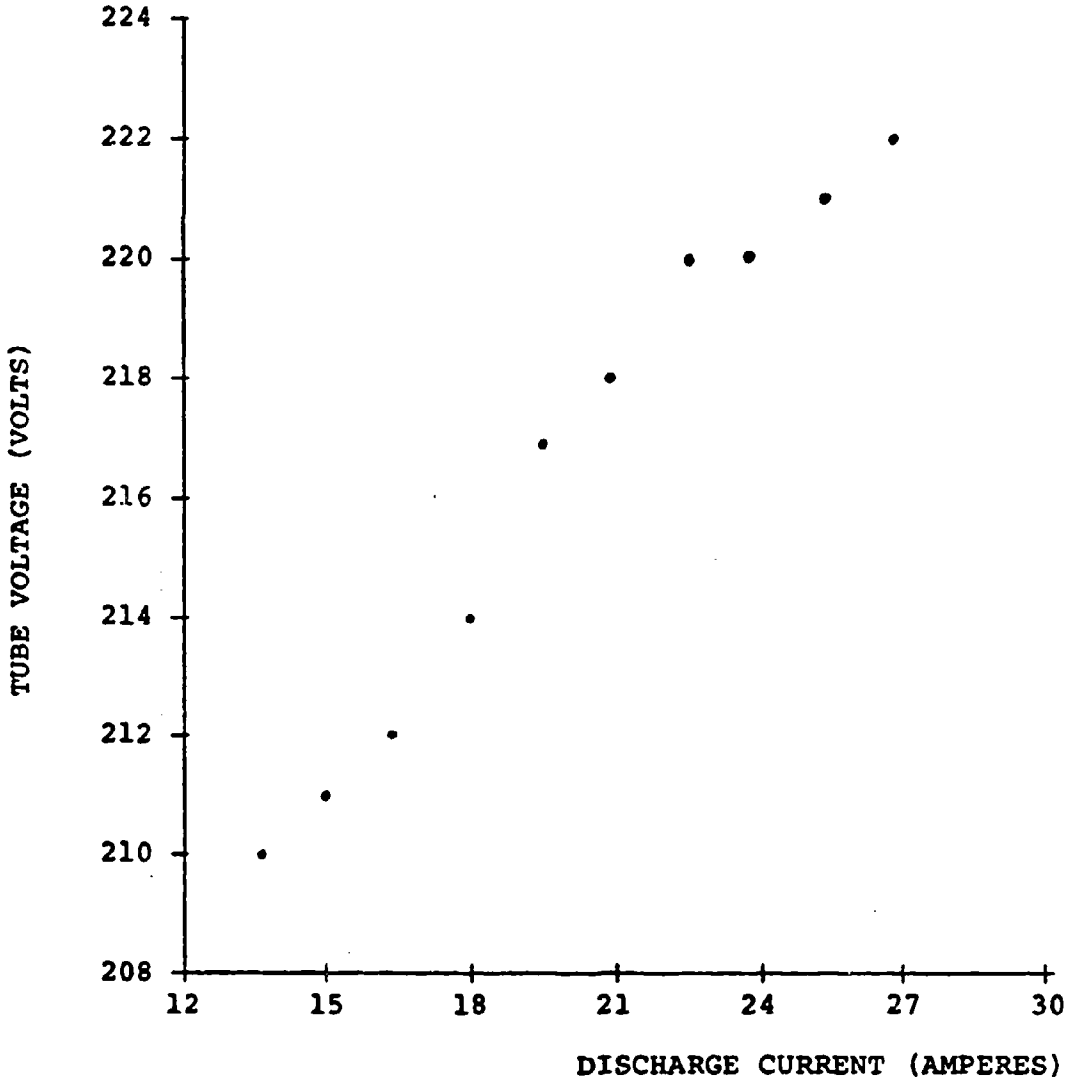

FIGURE II.4 - VOLTAGE/CURRENT RELATIONSHIP FOR THE LASER SCIENCES MODEL 254 DISCHARGE TUBE (ARGON PRESSURE = 1.0 TORR)

REFERENCES

[1] W. R. Bennett, Jr., P. J. Kindlmann, and G. N. Mercer, "Measurement of excited state relaxation rates," Appl. Opt. Suppl. 2, 34 (1965).

[2] W. R. Bennett, Jr, and P. J. Kindlmann, "Radiative and collision-induced relaxation of atomic states in the $2p^5 3p$ configuration of neon," Phys. Rev. 149, 38 (1966).

[3] A. J. DeMaria, W. H. Glenn, Jr., M. J. Briezna, and M.E. Mack, "Picosecond laser pulses," Proc. IEEE, 57, 2 (1969).

[4] P. W. Smith, "Mode-locking of laser," Proc. IEEE, 58, 1342 (1970).

[5] D. von der Linde, "Mode-locked lasers and ultrashort light pulses," Appl. Phys. 2, 281 (1973).

[6] A. J. DeMaria and D. A. Stetser, "Laser pulse-shaping and mode-locking with acoustic waves," Appl. Phys, Lett., 7, 71 (1965).

[7] W. R. Bennett, Jr., D. B. Carlin, and G. J. Collins, "Picosecond time-interval measurements and intensity correlations using the two-quantum photoelectic effect," IEEE J. Quantum Electronics, QE-10, 97 (1974).

[8] D. B. Carlin and W. R. Bennett, Jr., "Mode-locked, cavity-dumped laser design considerations," Appl. Opt., 15, 2020 (1976).

[9] H. Statz, F. A. Horrigan, S. H. Koozekanani, C. L. Tang, and G. F. Koster, "Transition probabilities for some Ar II laser lines," J. Appl. Phys., 36, 2278 (1965).
G. F. Koster, H. Statz, F. A. Horrigan, and C. L. Tang, 39, 4045 (1968).

[10] A. J. DeMaria, D. A. Stetser, and H. Heynau, "Self-mode-locking of laser with saturable absorber," Appl. Phys. Lett., 8, 174 (1966).

[11] H. W. Mocker and R. J. Collins, "Mode competition and self-locking effects in a Q-switched ruby laser," Appl. Phys. Lett., 7, 270 (1965).

[12] C. V. Raman and N. S. N. Nath, "The diffraction of light by high frequency sound waves: parts III, IV, and V," Proc. Ind. Acad. Sci., pp. 75, 119, 459 (1936).

[13]B. D. Cook and E. A. Hiedemann, "Diffraction of light by ultrasonic waves of various standing wave ratios," J. Acoust. Soc. Am., 33, 945 (1948).

[14]C. F. Quate, C. D. Wilkinson, and D. K. Winslow, "Interaction of light and microwave sound," Proc. IEEE, 53, 1604 (1965).

[15]W. R. Klein and B. D. Cook, "Unified approach to ultrasonic light diffraction," IEEE Trans. Sonics and Ultra-Sonics, SU-14, 123 (1967).

[16]S. I. Green, "50 picosecond detector laser pulse monitor," Rev. Sci. Instrum., 47, 1083 (1976).

[17]M. Maier, W. Kaiser, and J. A. Giordmaine, "Intense light bursts in the stimulated Raman effect," Phys. Rev. Lett., 17, 1275 (1966).

[18]J. A. Armstrong,"Measurement of picosecond laser pulse widths," Appl. Phys, Lett., 10, 16, (1967).

[19]H. P. Weber, "Generation and measurement of ultrashort light pulses," J. Appl. Phys., 39, 6041 (1968).

[20]A. Dienes, E. P. Ippen, and C. V. Shank, "A mode locked CW dye laser," Appl. Phys. Lett., 19, 258 (1971).

[21]E. P. Ippen, C. V Shank, and A. Dienes, "Passive mode locking of a CW dye laser," Appl. Phys. Lett., 21, 348 (1972).

[22]J. A. Giordmaine, P. M. Rentzepis, S. L. Shapiro, and K. W. Wech, "Two photon excitation of fluorescence by picosecond light pulses," Appl. Phys. Lett., 11, 216 (1967).

[23]H. P. Weber and H. G. Danielmeyer, "Multimode effects in intensity correlation measurements," Phys. Rev. A, 2, 2074 (1970).

[24]R. J. Glauber, "Optical coherence and photon statistics," In Quantum Optics and Electronics. New York: Gordon and Breach, 1964, pp. 65-185.

[25]W. R. Bennett, Jr., The Physics of Gas Lasers, Documents on Modern Physics. New York: Gordon and Breach, 1977, pp. 21-34, 62-83.

[26]R. C. Sze, Ph.D. Thesis, Yale University, 1970 (unpublished).

[27] R. C. Sze and W. R. Bennett, Jr., "Spontaneous-emission profiles of argon-ion laser transitions," Phys. Rev. A, 5, 837 (1972).

[28] E. I. Gordon, "A review of acoustooptical deflection and modulation devices," Proc. IEEE, 54, 1391 (1966).

[29] D. Maydan, "Acoustooptical pulse modulators," IEEE J. Quantum Electronics, QE-6, 15 (1970).

[30] D. Maydan, "Fast modulator for the extraction of internal laser power," J. Appl. Phys., 41, 1552 (1970).

[31] D. Maydan and R. B. Chesler, "Q-switching and cavity dumping of Nd:YAlG lasers," J. Appl. Phys., 42, 1031 (1971).

[32] R. H. Johnson, "Characteristics of acoustooptic cavity dumping in a mode-locked laser," IEEE J. Quantum Electronics, QE-9, 255 (1973).

[33] A. G. Fox and T. Li, "Resonant modes in a maser interferometer," Bell Syst, Tech. J., 40, 453 (1961).

[34] H. Kogelnik and Li, "Laser beams and resonators," Proc. IEEE, 54, 1312 (1966).

[35] R. J. Harrach, Appl. Phys Lett., 14, 148 (1969).

[36] W. R. Bennett, Jr., "Inversion mechanisms in gas lasers," Appl. Opt. Suppl. 2, 3 (1965).

[37] R. Arrathoon and D. A. Sealer, "Collisional and radiative relaxation of selected states in neon I and argon II," Phys. Rev. A, 4, 815 (1971).

[38] W. R. Bennett, Jr., P. J. Kindlmann, G. N. Mercer, and J. Sunderland, "Relaxation rates of the Ar^+ laser levels," Appl. Phys. Lett., 5, 158 (1964).

[39] W. R. Bennett, Jr., and R. C. Sze, "CW gain measurement in small-bore argon-ion laser discharges using a novel modulation technique," IEEE J. Quantum Electronics, QE-10, 908 (1974).

[40] W. R. Bennett, Jr., G. N. Mercer, P. J. Kindlmann, B. Wexler, and H. Hyman, "Direct electron excitation cross sections pertinent to the argon ion laser," Phys. Rev. Lett., 17, 987 (1966).

[41] B. van der Sijde, J. W. H. Dielis, and W. P. M. Graef, "Experimental natural lifetime determination of the Ar(II) lower laser levels," J. Quant. Spectrosc. Radiat. Transfer, 16, 1011 (1976).

[42] F. A. Korolyev, V. V. Lebedeva, A. E. Novik, and A. I. Odintsov, "Experimental determination of radiation lifetimes for Ar II and Kr II resonance levels," Opt. Spectrosc., 33, 435 (1972).

[43] P. Zory, "Single-frequency operation of argon ion lasers," IEEE J. Quantum Electronics, QE-3, 390 (1967).

[44] J. A. Myer, I. Itzkan, and E. Kierstead, "Dye lasers in the ultraviolet," Nature, 225, 544 (1970).

[45] I. B. Berlman, Handbook of Fluorescence Spectra of Aromatic Molecules. New York: Academic Press, 1971, pp. 166.

[46] E. K. Sittig, "Elastooptic light modulation and deflection," in Progress in Optics, vol. X, E. Wolf, ed. New York: American Elsevier, 1972, pp.231-290.

[47] L. E. Hargrove, R. L. Fork, and M. A. Pollack, "Locking of He-Ne laser modes induced by synchronous intracavity modulation," Appl. Phys. Lett., 5, 4 (1964).

[48] M. Born and E. Wolf, Principles of Optics. New York: MacMillan, 1964, second edition, pp. 593-610.

[49] N. W. McLachlan, Bessel Function for Engineers. London: Oxford Univ. Press, 1961, pp.56.

[50] B. L. Wexler, "Reliable starting technique for an ion laser tube with internal gas return bores," Rev. Sci. Inst., 43, 1853 (1972).